THESIS REPORT

Master's Degree

Adaptive Wavelet Based Image Coding

by H. Jafarkhani
Advisor: N. Farvardin

M.S. 94-2

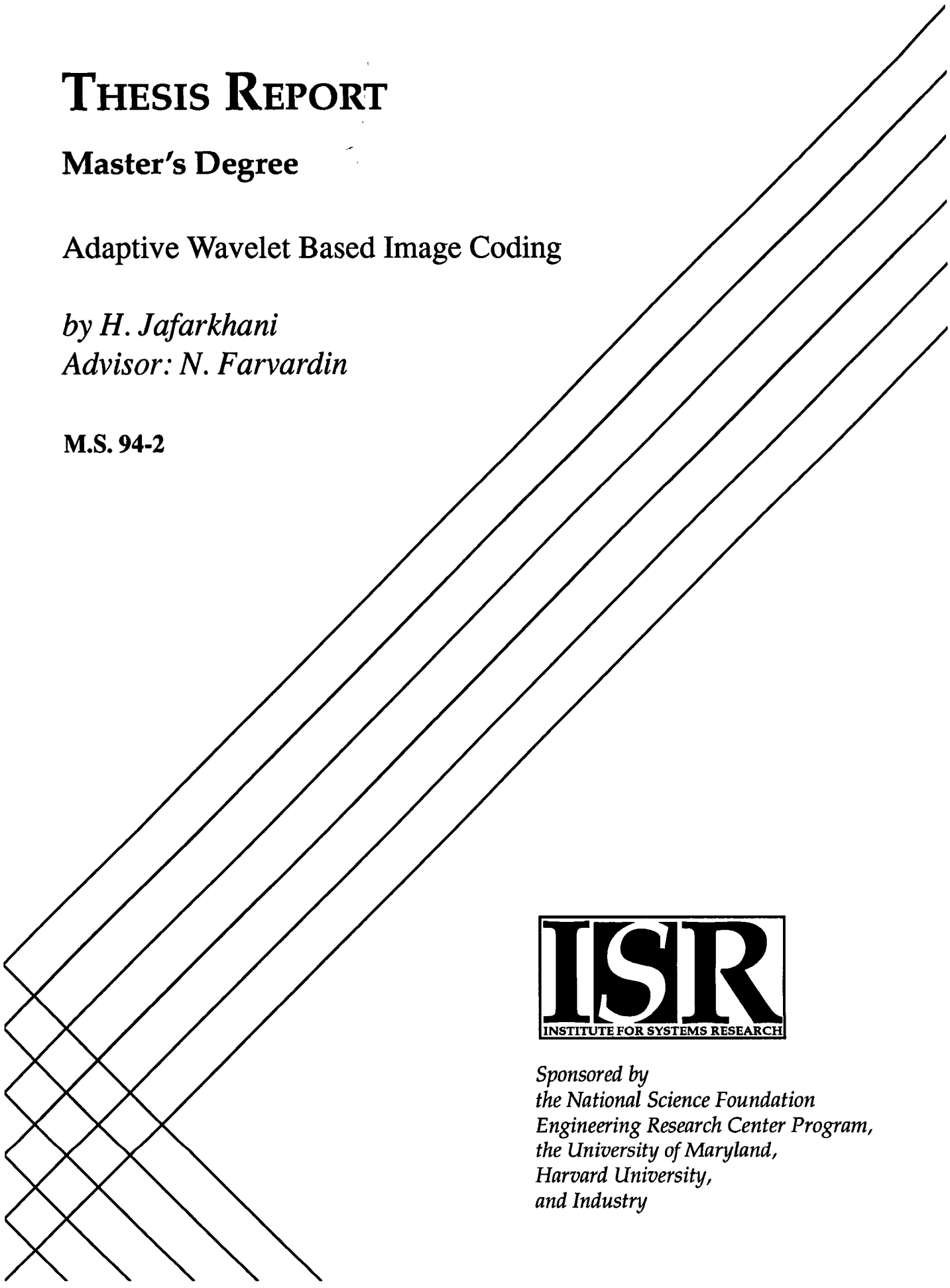

Sponsored by
the National Science Foundation
Engineering Research Center Program,
the University of Maryland,
Harvard University,
and Industry

Abstract

Title of Thesis: Adaptive Wavelet Based Image Coding

Name of degree candidate: Hamid Jafarkhani

Degree and year: Master of Science, 1994

Thesis directed by: Professor Nariman Farvardin
Department of Electrical Engineering

New schemes for classification of images are suggested. An application of these methods in adaptive DCT of images is considered. A new method to combine classification and bit allocation is introduced. Also, an efficient wavelet based image coding system using classification for adaptation is developed. Finally, practical considerations concerning overhead, complexity and performance are discussed.

Adaptive Wavelet Based Image Coding

by

Hamid Jafarkhani

Thesis submitted to the Faculty of the Graduate School
of The University of Maryland in partial fulfillment
of the requirements for the degree of
Master of Science
1994

Advisory Committee:

Professor Nariman Farvardin, Chairman/Advisor
Professor Rama Chellappa
Professor KuoJuey Ray Liu

How can you make someone leading his life so

patiently

solemnly

wondered;

stop.

F. F.

Acknowledgements

I would like to thank my advisor, Professor Nariman Farvardin, for his support, long discussions, numerous good ideas and encouragement. His mature scientific judgement has been the best help during the course of this work. Working with him has been my best educational experience.

I also want to thank Mrs. Paridokht Badakhshan for her hospitality during my first year of stay in the states.

My mother has always encouraged me to pursue higher education. She has been the first motivation behind my work. It is to her that I dedicate this thesis.

Table of Contents

Section	Page
List of Tables	vi
List of Figures	vii
1 Introduction	1
2 Subband Coding and Discrete Wavelet Transform(DWT)	4
2.1 Multiresolution Signal Decomposition	5
2.2 Biorthogonal Wavelet Bases	11
2.3 Extension to Two-dimensional Signals	13
3 Image Block Classification	17
3.1 Gain-Based Classification	18
3.1.1 Chen-Smith Approach	19
3.1.2 Equal-Normalized-Standard Deviation Approach	20
3.2 Combined Classification and Bit Allocation	22
3.3 Linear Prediction and Spectral Classification of Images	26
3.3.1 LPC Coding in Speech	27

3.3.2 Codebook Generation (VQ Design) 29
3.3.3 Application in Image Classification 32

4 Image Coding Using Adaptive Discrete Cosine Transform 39

4.1 Bit Allocation 42
4.2 Comparing Adaptation Schemes 44

5 Wavelet Coding of Images 49

5.1 Quantization of Low Frequency Subbands 51
5.2 Quantization of High Frequency Subbands 52
5.3 System Overhead 53
5.4 Simulation Results and Comparison 54

6 Conclusion 69

Bibliography 71

List of Tables

Number		Page
4.1	ADCT Simulation Results for the 512 × 512 LENNA.	46
5.1	Statistics of 16 Subbands of the 512 × 512 LENNA.	58
5.2	Simulation Results of Different Classification Schemes for the 512× 512 LENNA.	60
5.3	Comparing Different Block Sizes for the 512 × 512 LENNA. . . .	61

List of Figures

Number		Page
2.1	Multiresolution Approximation of $L^2(\mathbb{R})$	7
2.2	Implementation of the Biorthogonal Wavelet Scheme	10
2.3	Decomposing an Image into Four Subbands.	14
2.4	512×512 LENNA	15
2.5	Decomposed 512×512 LENNA	16
2.6	Enumerating Subbands of an Image.	16
3.1	Chen-Smith Classification Image for the 512×512 LENNA.	34
3.2	ENSD Classification Image for the 512×512 LENNA.	35
3.3	Sample Blocks.	36
3.4	LPC Analysis as a Two-step Process.	36
3.5	Spectral Classification Image for the 512×512 LENNA.	37
3.6	Gain-Spectral Classification Block Diagram.	38
4.1	ADCT Simulation Results for the 512×512 LENNA (block size $= 16$).	47

4.2 Reconstructed Images for the 512 × 512 LENNA (Rate = 0.25 Bits/Pixel): (a)Nonadaptive, (b)Spectral Classification, (c)Chen-Smith Classification and (d)ENSD Classification. 48

5.1 System Block Diagram. 51

5.2 Classification Image for the 512 × 512 LENNA Subbands. 59

5.3 Comparing Different Classification Schemes for the 512 × 512 LENNA. 60

5.4 Comparing Systems A, B and F for the 512 × 512 LENNA. 61

5.5 Comparing Systems B, C and F for the 512 × 512 LENNA. 62

5.6 Comparing Systems C, E and F for the 512 × 512 LENNA. 63

5.7 Comparing Systems D, E and F for the 512 × 512 LENNA. 64

5.8 Comparing Systems A, E and F for the 512 × 512 LENNA. 65

5.9 Comparing Systems E, F and G for the 512 × 512 LENNA. 66

5.10 Performance of Different Image Coding Systems for the 512 × 512 LENNA. 67

5.11 Reconstructed Images for System A (all rates in Bits/Pixel): (a)Rate = 0.25, (b)Rate = 0.5, (c)Rate = 0.75 and (d)Rate = 1.0. 68

Chapter 1

Introduction

The purpose of *Data Compression* is to represent a source by a rate lower than the original rate. The rate is defined as the average number of binary digits or bits needed for the representation. There are two kinds of data compression. The first one is noiseless or lossless compression in which the original information can be retrieved perfectly from the compressed data. Huffman coding, arithmetic coding and Ziv-Lempel coding are examples of noiseless coding systems. We define the compression ratio as $\frac{R_{original}}{R_{compressed}}$ where $R_{original}$ is the number of bits in the original signal and $R_{compressed}$ is the number of bits in the compressed version. Due to Shannon's source coding theorem, the compression ratio for noiseless coding systems is limited. To get higher compression ratios, we have no choice but to use lossy compression methods in which a perfect reconstruction of the source is impossible. The purpose of lossy compression is to obtain the "best possible quality" for a given rate. The best possible quality may have different meanings to different people. A quantitative measure of closeness is needed to compare different methods of data compression. This distortion measure should have some properties to be useful. It should be (i) mathematically tractable so as

to lend itself to analysis and (ii) subjectively meaningful so that large and small average distortion values correspond, respectively, to poor and good subjective qualities as perceived by the user of the data compression system. The smallest average distortion for a given rate is given by the source distortion-rate function [Ber71].

The most popular distortion measure is the squared-error distortion measure. The mean squared-error (MSE) between the source sequence $\{x_i\}$ and its reproduction $\{\hat{x}_i\}$ is defined by

$$MSE = \frac{1}{M}\sum_{i=1}^{M}(x_i - \hat{x}_i)^2$$

where M is the number of samples in the sequence. Although the squared-error criterion is not always perceptually meaningful, it has been used extensively for designing image compression systems. Using MSE for speech compression does not make sense because MSE is not invariant to shifts in time or space; however, delayed speech would sound as good as the original. The Itakura-Saito distortion measure [Ita68] is well behaved for speech compression applications. The same problem is valid for images; but, there is no good substitution available.

Digital image storage systems and digital image transmission are two growing applications of data compression. Some specific applications are the storage of medical images, digital video recording, video-phone, teleconferencing and the transmission of still pictures over telephone lines. The general problem is addressed by the field of image coding. Different image coding systems are available. Subband coding and transform coding are two popular techniques and have advantages and disadvantages compared to each other. The transform coding approach usually suffers from blockiness; however, it achieves higher compression ratios for the same amount of MSE. On the other hand, the subband coding

approach naturally gives some nice properties like spectral shaping of the quantization noise and progressive transmission of images in which increasingly better reproductions of the transmitted image can be reconstructed by the decoder.

In this thesis, we consider the effects of adaptation on the performance of transform and subband coding systems. Chapter 2 provides a brief description of subband coding and discrete wavelet transform. In Chapter 3, the problem of classification is considered and several solutions to the problem are suggested. An application of these methods in adaptive DCT of images is considered in Chapter 4. An efficient wavelet based image coding system using classification for adaptation is developed in Chapter 5 and practical considerations concerning overhead, complexity and performance are discussed. Chapter 6 consists of conclusions and suggestions for future research.

Chapter 2

Subband Coding and Discrete Wavelet Transform(DWT)

The idea of subband coding is to decompose the source into its different frequency subbands and encode each subband using a suitable coding system [Cro76a]. Because there is little correlation between the decomposed subbands, they can be coded separately [Mal89], [Ant92], [Tan92]. The separate coding of different subbands provides three desirable features. First, by allocating the available bits for encoding among the subbands and using an appropriate quantizer for each of them, the encoding process can be tailored to the statistics of each subband. Second, spectral shaping of the quantization noise is possible. This feature can be used to take advantage of the noise perception of the human auditory system for speech or the human visual system for images. Third, the subband decomposition of the signal spectrum leads naturally to multiresolution signal decomposition - a feature that is becoming increasingly important for the seamless communication networks of the future. This is also useful for progressive

transmission of images in which an increasingly higher resolution and quality image can be reconstructed by the decoder.

Using a bank of n band-pass filters, each associated with a separate frequency channel, n different subbands of the source will be created. A dual set of filters is needed to reconstruct the original source from its subbands. Quadrature Mirror Filters (QMF's) can be used to have a perfect reconstruction [Cro76b]. A multiresolution representation using wavelet orthonormal [Mal89] or biorthogonal [Ant92] bases is another approach which is the subject of this chapter.

In a subband coding system, after decomposition, the subbands are quantized and encoded. Therefore, it is not clear that the subband filters need to be perfect reconstruction filters. However, since no definitive techniques for combining the filter design and quantization are known, the filters used for decomposition are usually perfect reconstruction filters. Good coding results have been reported based on these filters.

2.1 Multiresolution Signal Decomposition

Defining $L^2(\mathbb{R})$ as the vector space of measurable and square-integrable one-dimensional (1-D) functions, wavelets are functions $\psi(x)$ whose translations and dilations ($\psi_{m,n}(x) = 2^{-m/2}\psi(2^{-m}x - n)$) can be used for the expansion of functions in $L^2(\mathbb{R})$ [Mey85]. The class of functions $\psi(x) \in L^2(\mathbb{R})$ that generate an orthonormal basis for $L^2(\mathbb{R})$ can be described using the multiresolution approach to wavelets [Mal89]. In what follows, the model is first described for 1-D functions and then extended to two dimensions for image processing applications.

Let A_m be a linear operator used to approximate a signal at resolution m.

Clearly, if $A_m f(x)$ is the approximation of $f(x) \in L^2(\mathbb{R})$ at resolution m, then $A_m(A_m f(x)) = A_m f(x)$. Thus, A_m is a projection operator on a particular vector space $V_m \subset L^2(\mathbb{R})$. The vector space V_m can be interpreted as the set of all possible approximations at resolution m of functions in $L^2(\mathbb{R})$. Any set of vector spaces $\{V_m\}$, for all m in $\mathbb{Z}$, which satisfies the following properties is called a multiresolution approximation of $L^2(\mathbb{R})$ [Mal89]:

$$V_m \subset V_{m-1}, \quad \forall m \in \mathbb{Z}, \tag{2.1}$$

$$f(x) \in V_m \Leftrightarrow f(2x) \in V_{m-1}, \quad \forall m \in \mathbb{Z}, \tag{2.2}$$

$$\exists \phi \in V_0 \text{ such that } \phi(x-n) \in V_0, \quad \forall n, \tag{2.3}$$

$$\bigcap_m V_m = \{0\}, \tag{2.4}$$

$$\bigcup_m V_m = L^2(\mathbb{R}). \tag{2.5}$$

Mallat has shown that for a multiresolution approximation of $L^2(\mathbb{R})$, there exists a unique function $\phi(x) \in L^2(\mathbb{R})$, called a *scaling function*, such that $\phi_{m,n}(x) = 2^{-m/2}\phi(2^{-m}x - n)$, $n \in \mathbb{Z}$ forms an orthonormal basis for V_m [Mal89]. The orthogonal projection of $f(x)$ on V_m can be computed by decomposing the signal $f(x)$ with the above orthonormal basis:

$$A_m f(x) = \sum_{n=-\infty}^{\infty} < f, \phi_{m,n} > \phi_{m,n}(x). \tag{2.6}$$

A discrete approximation of $f(x)$ at resolution m can be defined as

$$a_{m,n}(f) = A_m^n f =< f, \phi_{m,n} >, \quad \forall n \in \mathbb{Z}. \tag{2.7}$$

Equation (2.7) can be interpreted as a convolution product evaluated at point $2^m n$:

$$a_{m,n}(f) = A_m^n f = (f(u) * \phi_{m,0}(-u))(2^m n), \quad \forall n \in \mathbb{Z}. \tag{2.8}$$

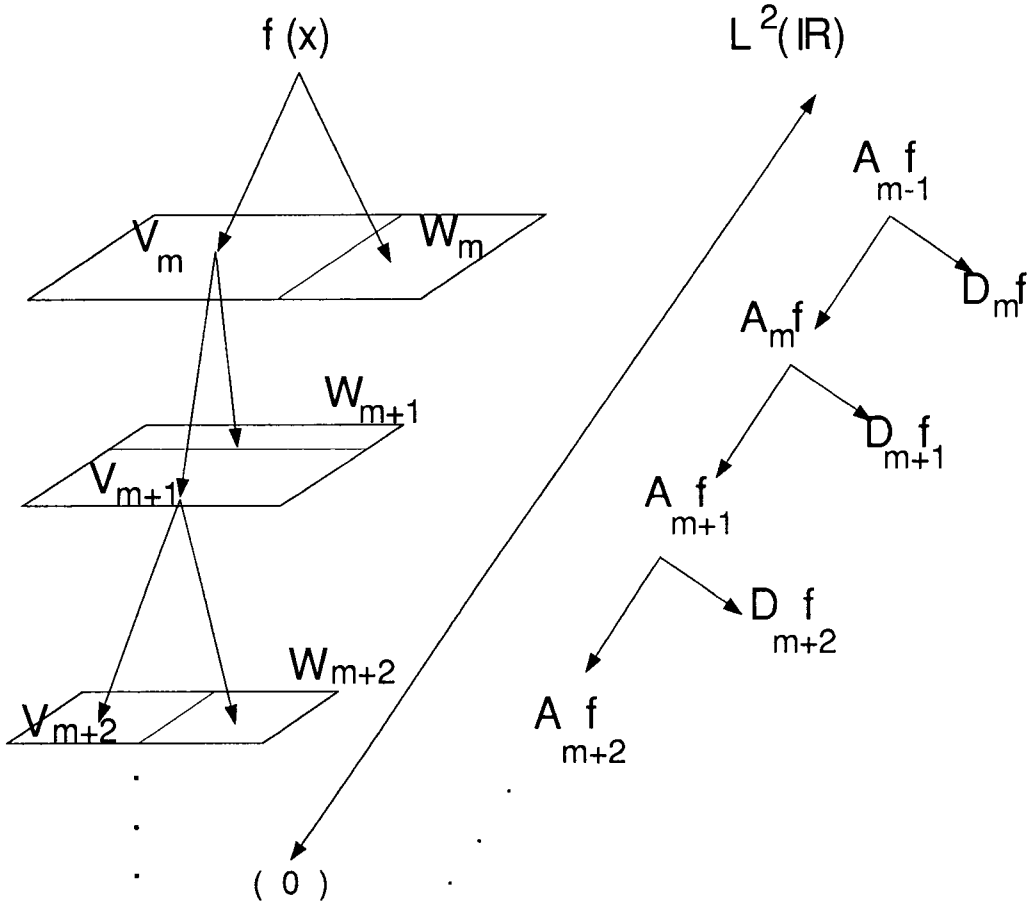

Figure 2.1: Multiresolution Approximation of $L^2(\mathbb{R})$

The above equation is also equivalent to low-pass filtering of $f(x)$ followed by a uniform sampling at the rate 2^m. To follow rapid changes of the signal in space domain as well as the frequency domain using finite number of coefficients, the transform used must accept nonstationarity and be well localized in both space and frequency domains [Ant92].

Let $\tilde{H}$ be a discrete filter with impulse response

$$\tilde{h}(n) = < \phi_{1,0}, \phi_{0,n} >, \tag{2.9}$$

and let H be the mirror filter with impulse response $h(n) = \tilde{h}(-n)$. It can be

shown that [Mal89]

$$a_{m,n}(f) = \sum_{k=-\infty}^{\infty} h(2n-k)a_{m-1,k}(f). \tag{2.10}$$

Equation (2.10) implies that $a_{m,n}(f)$ can be computed by convolving $a_{m-1,k}(f)$ with H and sub-sampling by 2. All the discrete approximations $a_{m,n}(f)$, for $m > 0$ can be computed from $a_{1,n}(f)$ by repeating this process. Usually a regularity condition is imposed on the scaling function requiring that $\phi(x)$ be continuously differentiable and that the asymptotic decay of $\phi(x)$ and $\phi\prime(x)$ satisfy

$$| \phi(x) | = O(x^{-2}), \tag{2.11}$$

and

$$| \phi\prime(x) | = O(x^{-2}). \tag{2.12}$$

Having the above conditions on $\phi(x)$, the filter H will satisfy the following properties:

$$h(n) = O(n^{-2}), \tag{2.13}$$

$$| H(0) | = 1, \tag{2.14}$$

and

$$| H(\omega) |^2 + | H(\omega+\pi) |^2 = 1. \tag{2.15}$$

The orthogonal complement subspace of V_m in V_{m-1} is denoted by W_m, i.e.

$$W_m \oplus V_m = V_{m-1} \text{ and } W_m \perp V_m. \tag{2.16}$$

The orthogonal projection of a signal on W_m is called the *detail signal* at resolution m.

Denoting the Fourier transform of $f(x)$ by $\hat{f}(\omega)$ and the conjugate of a complex number x by $\overline{x}$, $\psi(x)$ is a function defined by

$$\hat{\psi}(\omega) = \tilde{G}(\omega/2)\hat{\phi}(\omega/2), \tag{2.17}$$

where

$$\tilde{G}(\omega) = e^{-j\omega}\overline{\tilde{H}(\omega+\pi)}. \tag{2.18}$$

Then $\psi_{m,n}(x)$, for all n in $\mathbb{Z}$, is an orthonormal basis of W_m and $\psi_{m,n}(x)$, for all (m,n) in $\mathbb{Z}^2$, is an orthonormal basis of $L^2(\mathbb{R})$. Here, $\psi(x)$ is called an orthogonal mother wavelet. The orthogonal projection of $f(x)$ on W_m (detail signal) can be characterized by the following set of inner products:

$$c_{m,n}(f) = D_m^n f = < f, \psi_{m,n} >, \quad \forall n \in \mathbb{Z}. \tag{2.19}$$

Upon defining a filter $\check{G}$ with impulse response $\check{g}(n)$ given by

$$\check{g}(n) = < \psi_{1,0}, \phi_{0,n} >, \quad \forall n \in \mathbb{Z}, \tag{2.20}$$

it can be shown that

$$c_{m,n}(f) = \sum_{k=-\infty}^{\infty} g(2n-k)a_{m-1,k}(f), \tag{2.21}$$

where $g(n) = \check{g}(-n)$. The detail signal $c_{m,n}(f)$ can be computed by convolving $a_{m-1,n}(f)$ with the filter g and sub-sampling by 2. Using (2.18), $\check{g}(n)$ and $\tilde{h}(n)$ are related by the following equation:

$$\check{g}(n) = (-1)^{1-n}\tilde{h}(1-n). \tag{2.22}$$

The two filters $\check{G}$ and $\tilde{H}$ are referred to as QMF's and are high-pass and low-pass filters respectively.

In practice, a physical measuring device can only measure a signal at a finite resolution. For normalization purposes, we suppose that this resolution is equal to 1. The original discrete $a_{1,n}(f)$ measured at resolution 1 is represented by $a_{M,n}(f)$, $\{c_{m,n}(f)\}$, $1 < m \leq M$. This set of discrete signals is called an orthogonal wavelet representation. If the discrete approximation of the original signal at resolution 1 has N samples, then the discrete signals $c_{m,n}$ and $a_{m,n}$ each will have $2^{-m}N$ samples. Therefore, the wavelet representation has the same total number of samples as the original one. This is because of orthogonality.

Reconstruction can be achieved by upsampling (placing zeros between neighboring samples) $a_{m,n}(f)$ and $c_{m,n}(f)$ and passing them through $\tilde{H}$ and $\tilde{G}$ respectively:

$$a_{m-1,l}(f) = \sum_{n=-\infty}^{\infty} [\tilde{h}(l-2n)a_{m,n}(f) + \tilde{g}(l-2n)c_{m,n}(f)]. \tag{2.23}$$

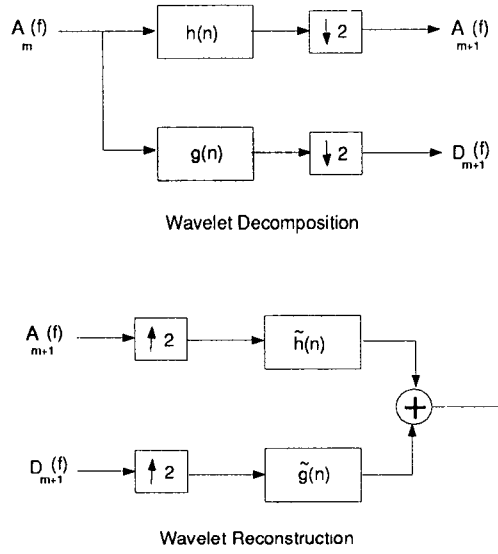

Figure 2.2: Implementation of the Biorthogonal Wavelet Scheme

2.2 Biorthogonal Wavelet Bases

Most of the orthonormal wavelet bases have infinitely supported ψ, corresponding to filters h and g with infinitely many taps. Having finite number of taps (using FIR filters) is required in practice and can be achieved when the support of ψ is finite. It is desirable that the FIR filters used be linear-phase, since such filters can be easily cascaded in a pyramidal filter structure without the need for phase compensation [Ant92].

Unfortunately, there are no nontrivial orthonormal linear-phase FIR filters with the exact reconstruction property. The only symmetric exact reconstruction filters are those corresponding to the Haar basis, i.e. $h_0 = h_1 = 2^{1/2}$ and $g_0 = -g_1 = 2^{1/2}$, with all other $g_n, h_n = 0$ [Mal89].

By preserving the linear-phase property of the FIR filters and relaxing the orthonormality requirement, and using biorthogonal bases, it is possible to have perfect reconstruction and arbitrarily high regularity [Ant92]. In such a scheme (Fig. 2.2), the decomposition is the same as before

$$c_{m,n}(f) = \sum_{k=-\infty}^{\infty} g(2n-k)a_{m-1,k}(f), \tag{2.24}$$

$$a_{m,n}(f) = \sum_{k=-\infty}^{\infty} h(2n-k)a_{m-1,k}(f). \tag{2.25}$$

However, reconstruction becomes

$$a_{m-1,l}(f) = \sum_{n=-\infty}^{\infty} [\tilde{h}(2n-l)a_{m,n}(f) + \tilde{g}(2n-l)c_{m,n}(f)], \tag{2.26}$$

where the filters $\tilde{h}$ and $\tilde{g}$ may be different from h and g. Perfect reconstruction is possible when

$$\tilde{g}(n) = (-1)^n h(1-n), \tag{2.27}$$

$$g(n) = (-1)^n \tilde{h}(1-n), \tag{2.28}$$

and

$$\sum_{n=-\infty}^{\infty} h(n)\tilde{h}(n+2k) = \delta_{k,0}. \tag{2.29}$$

The interpretation of the biorthogonal scheme in terms of the bases can be done as follows. Define the functions ϕ and $\tilde{\phi}$ by

$$\phi(x) = \sum_{n=-\infty}^{\infty} h(n)\phi(2x-n), \tag{2.30}$$

$$\tilde{\phi}(x) = \sum_{n=-\infty}^{\infty} \tilde{h}(n)\tilde{\phi}(2x-n). \tag{2.31}$$

Also define

$$\psi(x) = \sum_{n=-\infty}^{\infty} g(n)\phi(2x-n), \tag{2.32}$$

$$\tilde{\psi}(x) = \sum_{n=-\infty}^{\infty} \tilde{g}(n)\tilde{\phi}(2x-n). \tag{2.33}$$

Then $a_{m,n}(f)$ and $c_{m,n}(f)$ can be rewritten as

$$a_{m,n}(f) = < \phi_{m,n}, f >, \tag{2.34}$$

$$c_{m,n}(f) = < \psi_{m,n}, f > . \tag{2.35}$$

Reconstruction is done by

$$f = \sum_{m,n} < \psi_{m,n}, f > \tilde{\psi}_{m,n}. \tag{2.36}$$

Equation (2.36) is very similar to the orthonormal case. The only difference is that the expansion of f with respect to the basis $\tilde{\psi}_{m,n}$ uses the coefficients computed via the dual basis $\psi_{m,n}$.

2.3 Extension to Two-dimensional Signals

A simple way for extending the 1-D transform of the previous section to a 2-D case is by separating the horizontal and vertical orientations. A scaling function can be defined by

$$\phi(x,y) = \phi(x)\phi(y), \tag{2.37}$$

where $\phi(x)$ is a 1-D scaling function. Let $\psi(x)$ be the wavelet associated with the scaling function $\phi(x)$. Then, the three 2-D wavelets are defined as

$$\psi^H(x,y) = \phi(x)\psi(y), \tag{2.38}$$

$$\psi^V(x,y) = \psi(x)\phi(y), \tag{2.39}$$

$$\psi^D(x,y) = \psi(x)\psi(y). \tag{2.40}$$

The implementation is the same as before. Practically, rows will be decomposed by using the 1-D decomposition filters and then the columns of the output will be decomposed using the same system.

When an $M \times N$ image is processed, after the first stage of decomposition, two $M \times \frac{N}{2}$ images will be created. Each of them will go through the same process for the columns and resulting in four $\frac{M}{2} \times \frac{N}{2}$ images. Clearly, the total number of samples is the same as the original one. Thus, to prevent using extra memory, these four sub-images can be placed in the memory location of the original image as in Figure 2.3. The original image can be replicated by first performing the reconstruction operations on columns and then doing the same process on rows.

Each sub-image can be decomposed into new subbands using the same set of filters. The result for two levels of decomposition for the 512×512 monochrome

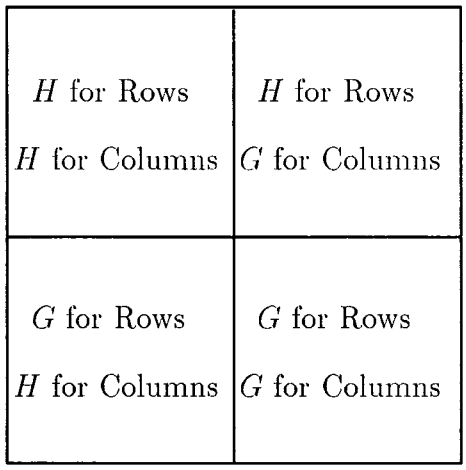

Figure 2.3: Decomposing an Image into Four Subbands.

Lenna image using the No. 2 7-9 spline filters in [Ant92] is shown in Figure 2.5. Also, we enumerate the subbands in Figure 2.6 for future use.

Figure 2.4: 512×512 LENNA

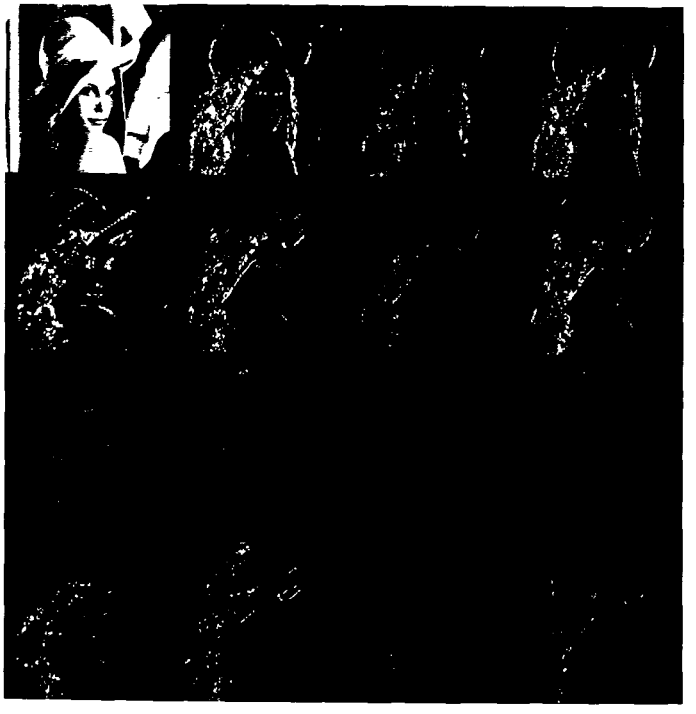

Figure 2.5: Decomposed 512 × 512 LENNA

1	5	9	D
2	6	A	E
3	7	B	F
4	8	C	G

Figure 2.6: Enumerating Subbands of an Image.

Chapter 3

Image Block Classification

In general, mapping a high-dimensional event space onto a low-dimensional feature space is called classification. A classified quantizer has separate codebooks for each of a set of classes [Ram86]. The motivation behind classified quantization is to design a separate codebook for specific events to do a better overall job of coding the source. Due to the apparent nonstationary behavior of the image blocks, classifying these blocks into more uniform regions provides the opportunity of using stationary probabilistic models for them. An example in image coding would be to have separate codebooks for edge areas and for shaded regions. Because the edge codebook is designed using only edges, it should better reproduce other edges. Additionally, using a nonuniform bit allocation among the different activity regions of the image, more bits can be assigned to the more important parts of the image. In this manner, the coding system captures the nonstationary behavior of the source and results in better performance.

The classification can be performed using a variety of methods such as decision trees, edge detection or vector quantization (VQ). Different approaches to the problem of image block classification are investigated below.

3.1 Gain-Based Classification

A suitable parameter for block classification is the gain (the square root of ac-energy) of image blocks. To compute the gains, the image is divided into $L \times L$ nonoverlapping blocks of pixels. If the $L \times L$ matrix which contains the pixels in the k^{th} block is denoted by A_k, its gain, g_k, is given by

$$g_k = \sqrt{\frac{1}{L^2} \sum_{i=1}^{L} \sum_{j=1}^{L} [A_k(i,j) - m_k]^2}, \tag{3.1}$$

where

$$m_k = \frac{1}{L^2} \sum_{i=1}^{L} \sum_{j=1}^{L} A_k(i,j). \tag{3.2}$$

This gain is a good measure of the level of activity in the block. For example, if the block only consists of one grey level, the corresponding gain is zero. On the other hand, when grey levels change rapidly in a block, its gain is relatively high. The extreme case is when half of the pixels are white (grey level 255) and the other half are black (grey level 0) and the corresponding gain is 127.5.

In gain-based classification schemes, blocks are classified into a prescribed number of classes according to their gain values. In this manner, blocks with close gain values are gathered in the same class. The classification procedure therefore assigns a class index to each block. A matrix whose entries are these class indices is referred to as the *classification table*. Needless to say, different criteria for classification result in different classification tables. In this section, we consider different criteria for classifying the blocks of an image based on their gain values.

3.1.1 Chen-Smith Approach

Chen and Smith [Che77] suggested a simple method to perform the classification, or, equivalently, to choose thresholds between the gain values of different classes. In this approach, thresholds are chosen such that all classes have the same number of blocks. If there are N blocks to be classified to k classes, the $\frac{N}{k}$ blocks with highest gain values fall into the first class. The $\frac{N}{k}$ blocks with highest gain values among the remaining blocks fall into the second class and so on. These class indices specify the classification table and can be coded using $\log_2 k$ bits/block. The classification table using four classes for the 512×512 Lenna image and blocks of size 16×16 is shown in Figure 3.1 in the form of an image. This image is constructed by assigning a different grey level to each class in order to visualize the classification table. Class 0 (low activity class) is represented by a grey value equal to 0. Classes 1, 2 and 3 are represented by grey levels 100, 150 and 255, respectively.

The Chen-Smith classification procedure is an easy way to classify blocks into different regions of activity. Although we have not defined a measurable quantity to compare classification schemes with each other, intuitively, there are situations in which this simple approach does not work well. For example, an image containing a large area with constant grey levels has a lot of blocks with zero (or very small) gains. If the number of such blocks exceeds $\frac{N}{k}$, the Chen-Smith procedure will put some of them into other classes although it is expected to have all of them in one class. The capability of allowing a different number of blocks in each class can potentially improve the classification. Also, as a gain-based classification method, Chen-Smith scheme pays no attention to the spectral shape of the blocks. This issue is considered in depth in Section 3.3.

3.1.2 Equal-Normalized-Standard Deviation Approach

In what follows we propose a different method in which after sorting the gain values, they are split into the given number of classes such that the mean-normalized standard deviation of the resulting classes are the same. The idea behind this approach is to allow the possibility of having a different number of blocks in each class and to have similar statistical properties within each class such that the representation of the blocks as one class is meaningful from a coding stand point. For a stationary source, standard deviation is a measure of dispersion of samples and the smaller is the standard deviation of a source, the denser will be the samples about the mean. When one of the classes has a higher dispersion than others, the blocks in that particular class do not have the same level of activity. Having the same density for different classes is considered as being more uniform inside classes.

Because of the discrete nature of the problem an exact solution for the problem may not be possible and there is no guarantee that a solution, if one exists, is unique. However, for practical purposes we try to make the mean-normalized standard deviation of the classes as close to each other as possible. For simplicity, for the moment, we consider the case with two classes. When there are N blocks sorted in an increasing order of their gain values g_i, $i = 1, 2, \ldots, N$, we look for an integer N' such that blocks 1 to N' belong to the first class and the remaining blocks belong to the second class. The mean m and standard

deviation σ of each class is defined by

$$\begin{aligned} m_1 &= \frac{1}{N'} \sum_{n=1}^{N'} g_n \\ m_2 &= \frac{1}{N-N'} \sum_{n=N'+1}^{N} g_n \\ \sigma_1^2 &= \frac{1}{N'} \sum_{n=1}^{N'} (g_n - m_1)^2 \\ \sigma_2^2 &= \frac{1}{N-N'} \sum_{n=N'+1}^{N} (g_n - m_2)^2. \end{aligned} \tag{3.3}$$

Here, N' is chosen such that

$$q_1 = \frac{\sigma_1}{m_1} = \frac{\sigma_2}{m_2} = q_2. \tag{3.4}$$

An iterative algorithm to find N' satisfying (3.4) is provided below. If there is no integer N' which solves (3.4), the algorithm finds the N' which minimizes $\mid q_1 - q_2 \mid$.

- *Algorithm*:

  1. Choose an initial value for N' (e.g. $N' = N/2$) and set the iteration number $i = 0$. Also choose i_{max} as an upper limit on the number of iterations.

  2. Compute q_1 and q_2 using (3.4) and set $i = i + 1$.

  3. If $\frac{\mid q_1 - q_2 \mid}{q_1} < \delta$ or $i > i_{max}$ stop. Otherwise,

     if $q_1 < q_2$, set $N' = N' + \Delta N'$

     if $q_1 > q_2$, set $N' = N' - \Delta N'$

     and go to (2).

To have a fast convergence, a large $\Delta N'$ can be chosen at the beginning of the algorithm and as the iteration number increases $\Delta N'$ must be decreased to one gradually.

The same algorithm can be generalized for a larger number of classes. For the case of M classes, M ratios $q_i = \frac{\sigma_i}{m_i}$, $i = 1, 2, \ldots, M$ and $(M-1)$ thresholds are needed. The algorithm is stopped when $\frac{\max_i q_i - \min_i q_i}{\min_i q_i} < \delta$ or when the number of iteration exceeds its maximum. At each step of the algorithm, the threshold corresponding to the class with maximum or minimum q_i is adjusted one after the other. The resulting classification image using four classes for the 512×512 Lenna ($\delta = 0.01$) is illustrated in Figure 3.2. In Figure 3.2, we have used the same grey levels as in Figure 3.1. Although it is not conclusive by itself, comparing Figures 3.1 and 3.2 shows that the equal-normalized-standard deviation (ENSD) classification is more successful than the Chen-Smith classification in separating high activity regions from other parts of the image. For example, using the Chen-Smith scheme results in putting the blocks corresponding to the strong edges and most of the blocks corresponding to the texture in the feather in the same class. On the other hand, using ENSD approach has placed these blocks into different classes.

3.2 Combined Classification and Bit Allocation

In this section, we will consider the possibility of approaching the problem of classification in a more general setup. One of the purposes of classification is to allocate bits nonuniformly among the different portions of a nonstationary source so as to best utilize the bit rate budget. A suitable encoder is designed for each class to minimize the distortion between the source and its quantized version. If a k-dimensional VQ is used for encoding each class, the rate-distortion

performance of the quantizer for high rates using the squared-error criterion can be formulated as [Ger79]

$$d_i(r_i) = \sigma_i^2 2^{-2r_i} \parallel p_i' \parallel_{\frac{k}{k+2}} , \tag{3.5}$$

where σ_i^2 is the variance of blocks in class i, $p_i(x)$ is the k-dimensional pdf of blocks in class i, $p_i'(x)$ is the variance normalized version of $p_i(x)$ and r_i is the rate of quantization in bits/vector. The ultimate purpose of bit allocation is to optimally assign bits among quantizers such that the overall distortion is minimized. The problem of bit allocation is considered in Section 4.1. In this section, we consider classification and bit allocation problems together and suggest a locally optimum algorithm to solve the combined problem. When the pmf of classes is denoted by $\{P_i\}$, we are interested in the classifier which solves the following problem:

$$\min \ D = \sum_{i=1}^{M} P_i \sigma_i^2 \ 2^{-2r_i} \parallel p_i' \parallel_{\frac{k}{k+2}}, \tag{3.6a}$$

$$\text{subject to} \sum_{i=1}^{M} P_i r_i = R. \tag{3.6b}$$

Our objective is to find the best set of thresholds for classification and the best values for rates, r_i's, simultaneously. The problem can be solved iteratively using the following steps:

1. For fixed thresholds, find the best rates, r_i's.

2. For fixed rates, find the best thresholds.

The algorithm is stopped when the relative change of D is less than a prescribed small value.

The constrained problem, in the first step of the algorithm, can be converted to an unconstrained one using a Lagrange multiplier as follows

$$J(\lambda) = \sum_{i=1}^{M} P_i \sigma_i^2 \; 2^{-2r_i} \parallel p_i' \parallel_{\frac{k}{k+2}} + \lambda \sum_{i=1}^{M} P_i r_i. \tag{3.7}$$

Taking derivative with respect to r_i and setting it to zero yields

$$-2 \ln 2 \; P_i \sigma_i^2 \; 2^{-2r_i} \parallel p_i' \parallel_{\frac{k}{k+2}} + \lambda P_i = 0, \; i = 1, 2, \ldots, M. \tag{3.8}$$

Solving for r_i's implies

$$r_i = \frac{1}{2} \log_2 [\frac{2 \ln 2 \; \sigma_i^2 \parallel p_i' \parallel_{\frac{k}{k+2}}}{\lambda}], \; i = 1, 2, \ldots, M, \tag{3.9}$$

or,

$$r_i = \lambda' + \log_2 \sigma_i + \frac{1}{2} \log_2 \parallel p_i' \parallel_{\frac{k}{k+2}}, \; i = 1, 2, \ldots, M, \tag{3.10}$$

where $\lambda' = \frac{1}{2} \log_2 \frac{2 \ln 2}{\lambda}$. Using the constraint, λ' can be calculated by

$$\sum_{i=1}^{M} P_i r_i = R = \lambda' + \sum_{i=1}^{M} P_i [\log_2 \sigma_i + \frac{1}{2} \log_2 \parallel p_i' \parallel_{\frac{k}{k+2}}], \tag{3.11}$$

or,

$$\lambda' = R - \sum_{i=1}^{M} P_i [\log_2 \sigma_i + \frac{1}{2} \log_2 \parallel p_i' \parallel_{\frac{k}{k+2}}]. \tag{3.12}$$

Substituting for λ' gives the final solution for r_i's:

$$\begin{aligned} r_i = \; & R - \textstyle\sum_{j=1}^{M} P_j [\log_2 \sigma_j + \frac{1}{2} \log_2 \parallel p_j' \parallel_{\frac{k}{k+2}}] + \\ & \log_2 \sigma_i + \tfrac{1}{2} \log_2 \parallel p_i' \parallel_{\frac{k}{k+2}}, \; i = 1, 2, \ldots, M. \end{aligned} \tag{3.13}$$

Assuming fixed $\parallel p_j' \parallel_{\frac{k}{k+2}}$ for all classes makes the computations much simpler:

$$r_i = R - \sum_{j=1}^{M} P_j \; \log_2 \sigma_j + \log_2 \sigma_i, \quad i = 1, 2, \ldots, M. \tag{3.14}$$

However since the allocated rates must be nonnegative, it may not always be possible to find a solution of this form. Although the rate-distortion model in

(3.5) works for high rates and therefore it is expected to get nonnegative rates from (3.14), even if some of the $r_i's$ in (3.14) are negative using Kuhn-Tucker conditions we still can solve the problem [Ort70]. The solution contains rates such that

$$r_i = (v + \log_2 \sigma_i)^+, \quad i = 1, 2, \ldots, M, \tag{3.15}$$

where v is chosen so that

$$\sum_{i=1}^{M} P_i (v + \log_2 \sigma_i)^+ = R. \tag{3.16}$$

Here $(x)^+$ denotes the positive part of x, i.e.

$$(x)^+ = \begin{cases} x & x > 0, \\ 0 & x \leq 0. \end{cases} \tag{3.17}$$

The process of finding v is called "water filling" process in which after sorting all $(\log_2 \sigma_i)$'s, we pick the largest one and by putting the $(v + \log_2 \sigma_i)^+ = 0$ for other classes, we find the v which solves (3.16). If the resulting v gives negative values for other $(v + \log_2 \sigma_i)$ quantities, it is the solution. Otherwise, we need to consider the second rate nonnegative and repeat the same procedure. Increasing the number of nonzero rates, the solution is achieved when the assumption of having zero rates is consistent with nonpositive values for $(v + \log_2 \sigma_i)$ [Ort70].

In the second step of the algorithm, by assigning r_i bits/vector to class i, we want to choose a set of thresholds to minimize D. This is an unconstrained minimization problem and can be solved using methods like Steepest-Descent or simulated annealing.

There is no simulation result available at the moment. At each step of the algorithm, the overall distortion, D, is decreased. Since D is a nonnegative number and a lower bounded nonincreasing sequence of numbers converges to a nonnegative number, the algorithm achieves a locally minimum D. In other words, the

algorithm is locally optimum and should outperform other schemes discussed in previous sections following an optimal bit allocation procedure. There is no proof for the uniqueness of the result and the goodness of the local optimum usually depends on the initial values. A full study of the tradeoffs between the complexity of the system and the amount of the improvement is needed to justify the use of the combined system.

3.3 Linear Prediction and Spectral Classification of Images

Gain-based classification uses the ac-energy level of each block as a measure of block activity. Based on this measure, the classifier divides the blocks into different activity regions. Although the performance of gain-based classifiers are usually good, there are some dissimilar cases which are not separable using this approach. For example, Figure 3.3 shows three blocks containing white and black strips. In two of them the strips are horizontal and in the other one vertical. The gain value of these blocks are the same and hence the gain-based classifier puts them in the same class although from a spectral point of view they are completely different.

Spectral properties of the signal is another feature which can, and perhaps must, be used for classification. For the example of Figure 3.3, the spectrum of the blocks in horizontal and vertical directions are different. In spectral classification, segments of a signal are classified into different classes based on their spectrum. Linear prediction coefficients are a good measure for representing spectral behavior of a signal. VQ can be used to split the spectral space into a

finite number of regions. An appropriate distortion measure for designing a VQ for this application is described below. This approach was first developed for quantization of speech spectral parameters [Buz80].

3.3.1 LPC Coding in Speech

A sequence of fixed-length segments of speech waveform called frames might be modeled as an autoregressive (AR) process. As a result, the coefficients of the all-pole filter and the corresponding input of the filter, called the excitation sequence, can be transmitted instead of quantizing and transferring the speech waveform. In practice, some information about the input of the filter is sent and the required excitation sequence is generated at the receiver. The speech waveform can be synthesized by constructing the same all-pole filter and applying the generated input to the filter [Mar76].

Suppose an M^{th}-*order* filter, $H(z)$, is given by

$$H(z) = \sigma/A(z) \quad \text{where} \quad A(z) = \sum_{i=0}^{M} a_i' z^{-i} \quad \text{with} \quad a_0' = 1. \tag{3.18}$$

Coefficients a_i', $i = 1, \ldots, M$ are called the linear prediction coefficients (LPC's). These coefficients are chosen such that the squared-error α between the original sequence $x(n)$ and the predicted signal $y(n) = \hat{x}(n)$ is minimized. The best autoregressive model using the above criterion can be found by solving the following system of M simultaneous equations known as Wiener-Hopf equations [Hay91]:

$$\sum_{i=0}^{M} a_i' r(\mid i - j \mid) = 0, \quad j = 1, 2, \ldots, M, \tag{3.19}$$

where $r(l)$ is the l^{th} autocorrelation coefficient of $x(n)$. There is also a simple iterative algorithm known as the Levinson-Durbin algorithm or the partial cor-

relation coefficients (PARCOR) algorithm to compute the parameters [Hay91]. The corresponding squared-error is

$$\alpha_M = \sigma^2 = \sum_{i=0}^{M} a_i r(i), \tag{3.20}$$

where α_M shows the minimum squared-error corresponding to an optimal M^{th}-*order* filter and $a_i,\ i = 1, \ldots, M$ are the optimum LPC's.

If the input of the filter $e(n)$ is an excitation sequence with autocorrelation $r_e(n) = \delta(n)$, the first M autocorrelations of $y(n)$ are the same as those of $x(n)$. This observation implies that the power spectrum of $H(z)$ defined by $\frac{\sigma^2}{|A(z)|^2_{z=e^{j\omega}}}$ is the same as the power spectrum of $x(n)$ (defined by $S_X(\omega) = \mid X(z) \mid^2_{z=e^{j\omega}}$) [Mar76].

In a derivation of linear prediction based on the concept of maximum likelihood, Itakura and Saito showed that finding the optimum predictor is equivalent to minimizing the quantity $D = d(\mid X \mid^2, \mid H \mid^2) = \int_{-\pi}^{\pi}[p(\theta) - \ln p(\theta) - 1]d\theta/2\pi$ where $p(\theta) = \mid \frac{X(\theta)}{H(\theta)} \mid^2$ [Ita68]. In other words, the problem at hand is equivalent to finding the filter $A(z)$ which minimizes the Itakura-Saito distortion measure. The Itakura-Saito distortion has some nice properties and can be computed in the time-domain as

$$D = \frac{1}{\sigma^2} \sum_n r_a(n) r_x(n) + \ln \frac{\sigma^2}{\alpha_\infty} - 1, \tag{3.21}$$

where $r_a(n) = \sum_k a_k a_{k+n}$ and α_∞ is the squared-error resulting from the optimum infinite-order filter.

Like other known distortion measures, $d(\mid X \mid^2, \mid H \mid^2)$ is zero if and only if $H(\omega) = X(\omega)$. Usually distortion measures satisfy the "triangular inequality." However, a very interesting property of the Itakura-Saito distortion is the

"triangular equality":

$$d(|X|^2, |H|^2) = d(|X|^2, |H_M|^2) + d(|H_M|^2, |H|^2), \tag{3.22}$$

where H_M is the optimal M^{th}-*order* autoregression filter for X and H is any arbitrary all-pole filter [Buz80]. The triangular equality enables us to combine the LPC computation procedure with the quantization of the LPC parameters. Traditionally, speech coding systems are based on a two-step process (Fig. 3.4). The first step is an identification process which computes the LPC's for each frame of speech; the second step quantizes the LPC's. The identification step uses the Itakura-Saito distortion (implicitly), so it is wise to use this distortion for the quantization step as well. Using the Itakura-Saito distortion, the overall distortion $d(|X|^2, |H|^2)$ can be minimized directly in one step instead of first obtaining $H_M(z)$ and then minimizing $d(|H_M|^2, |H|^2)$. This property is because of the triangular equality (3.22). The corresponding design procedure is described in the following section.

3.3.2 Codebook Generation (VQ Design)

The Generalized Lloyd algorithm is an iterative algorithm for designing a locally optimal VQ [Lin80]. The basic idea is to start from an initial codebook and iteratively improve the codebook in terms of a given distortion measure. The first step of the algorithm consists of finding the best partition of the space for a given codebook (Generalized Nearest Neighbor Rule). The second step obtains the best codebook for a given partition of the space (Generalized Centroid Rule). Because at each step of the algorithm the average distortion could not be larger than the previous one, convergence to a locally optimum quantizer is guaranteed.

The process will be terminated when the rate of improvement is less than a prescribed small value.

Generalized Nearest Neighbor Distortion Calculations

Since α_∞ depends only on the speech frame, minimizing $d(|\ X\ |^2, |\ H\ |^2)$ is equivalent to finding the $H(z) = \frac{\alpha}{A(z)}$ which minimizes

$$d(|X|^2, |H|^2) + 1 + \ln \alpha_\infty = \frac{\alpha}{\sigma^2} + \ln\ \sigma^2. \tag{3.23}$$

For each single frame of speech, the residual energy α must be computed as follows:

$$\alpha = \sum_{n=-\infty}^{\infty} r_a(n) r_x(n) = r_a(0) r_x(0) + 2 \sum_{n=1}^{M} r_a(n) r_x(n), \tag{3.24}$$

where

$$r_a(n) = \sum_{k=0}^{M-n} a_k a_{k+n},\ n = 0, 1, \ldots, M. \tag{3.25}$$

For computational efficiency, the transmitter codebook should probably contain the normalized sequence $\{\frac{r_a(n)}{\sigma^2},\ n = 0, 1, \ldots, M\}$ as well as the value of $\ln\ \sigma^2$. For a data sequence which is truncated to $n = 0, 1, \ldots, N-1$ samples, the standard short-term autocorrelation sequence, $r_x(n)$, is given by

$$r_x(n) = \sum_{k=0}^{N-1-n} x_k x_{k+n},\ n = 0, 1, \ldots, M < N. \tag{3.26}$$

Here, $\frac{\alpha}{\sigma^2} + \ln\ \sigma^2$ must be evaluated for each entry in the codebook and the vector with the smallest $\frac{\alpha}{\sigma^2} + \ln\ \sigma^2$ is chosen as the codevector.

Generalized Centroid Calculations

The sum of frame distortions can be calculated by

$$D = \sum_{k=1}^{L} d(|X_k|^2, |H|^2). \tag{3.27}$$

Using the definition of Itakura-Saito distortion, (3.21) implies

$$d(|X_k|^2, |H|^2) = \frac{\alpha^k}{\sigma^2} + \ln \sigma^2 - \ln \alpha_\infty^k - 1$$
$$= \frac{1}{\sigma^2} \int_{-\pi}^{\pi} |X_k|^2 |A|^2 \frac{d\theta}{2\pi} + \ln \sigma^2 - \int_{-\pi}^{\pi} \ln |X_k|^2 \frac{d\theta}{2\pi} - 1, \tag{3.28}$$

where α^k is the error corresponding to the k^{th} frame. By summing from $k = 1$ to $k = L$, we get

$$D = \frac{L}{\sigma^2} \int_{-\pi}^{\pi} |\overline{X}|^2 |A|^2 \frac{d\theta}{2\pi} + L \ln \sigma^2 - \int_{-\pi}^{\pi} \sum_{k=1}^{L} \ln |X_k|^2 \frac{d\theta}{2\pi} - L, \tag{3.29}$$

where

$$|\overline{X}|^2 = \frac{1}{L} \sum_{k=1}^{L} |X_k|^2 . \tag{3.30}$$

Therefore, D is given by

$$D = L\, d(|\overline{X}|^2, |G|^2) + u, \tag{3.31}$$

where

$$d(|\overline{X}|^2, |G|^2) = \frac{1}{\sigma^2} \int_{-\pi}^{\pi} |\overline{X}|^2 |A|^2 \frac{d\theta}{2\pi} + \ln \sigma^2 - \int_{-\pi}^{\pi} \ln |\overline{X}|^2 \frac{d\theta}{2\pi} - 1, \tag{3.32}$$

and

$$u = L \int_{-\pi}^{\pi} [\ln |\overline{X}|^2 - \frac{1}{L} \sum_{k=1}^{L} \ln |X_k|^2] \frac{d\theta}{2\pi}. \tag{3.33}$$

Equation (3.33) shows that u is a constant which is independent of $H(z)$. Therefore, finding a filter which minimizes D is equivalent to minimizing

$$\frac{D - u}{L} = d(|\overline{X}|^2, |G|^2). \tag{3.34}$$

This is the problem of minimizing the Itakura-Saito distortion and as it was claimed in Section 3.3.1, we have a standard linear prediction problem for modeling the average spectrum.

The autocorrelation sequences for all speech frames can be averaged to find an average autocorrelation sequence and then by solving the Wiener-Hopf equations for this sequence the coefficients of $H(z) = \frac{\sigma}{A(z)}$ can be calculated. These coefficients represent the generalized centroid of the frames.

3.3.3 Application in Image Classification

A VQ based on the Itakura-Saito distortion measure can be used to classify image blocks. We refer to this approach as spectral classification because spectral contents of the blocks are used to divide them into different classes. An image is a 2-D signal and the VQ developed in Section 3.3.2 works for 1-D signals. Zigzag scanning can be used to convert the 2-D blocks of an image into 1-D sequences [Pea90].

In spectral classification, the image is divided into 2-D blocks and each block is zigzag scanned to create a 1-D version of the signal. Using a large training sequence of monochrome images, a VQ is designed as was described in Section 3.3.2. The resulting codebook is used to classify blocks of an image outside the training sequence. The classification image for the 512×512 Lenna using 16×16 blocks and a 10^{th}-order filter is shown in Figure 3.5. In Figure 3.5, we have used the same grey levels as Figures 3.1 and 3.2. It is clear from Figure 3.5 that spectral classification is successful in separating regions with different levels of activity from each other. Making a reasonable conclusion as to the efficacy of the classification scheme should be based on the final results of the coding system. At this point, we can only consider the capability of a classification scheme in separating active regions from smooth regions of an image. From this point of view, spectral classification seems to perform better than other classification

schemes. In the next chapter, we design an image compression system based on the idea of block classification and compare the performance of the classification schemes with each other.

Also a combination of gain-based classification and spectral classification can be used. Figure 3.6 shows a block diagram of such a scheme. In Figure 3.6, K_1 gain classes and K_2 spectral classes are used to classify N^2 blocks of an image. Therefore, the image blocks are divided into K_1K_2 classes. In this scheme, first, we classify the blocks of an image based on the gain values. Then, each gain class is further classified based on the spectral characteristics of the blocks. A separate VQ is designed for each gain class and as it is shown in the block diagram the gain index is used to select the appropriate VQ.

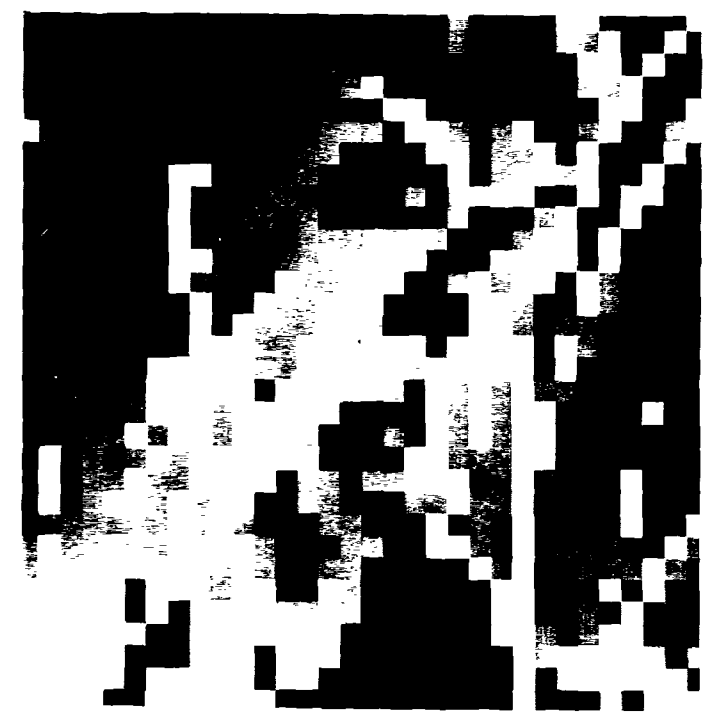

Figure 3.1: Chen-Smith Classification Image for the 512×512 LENNA.

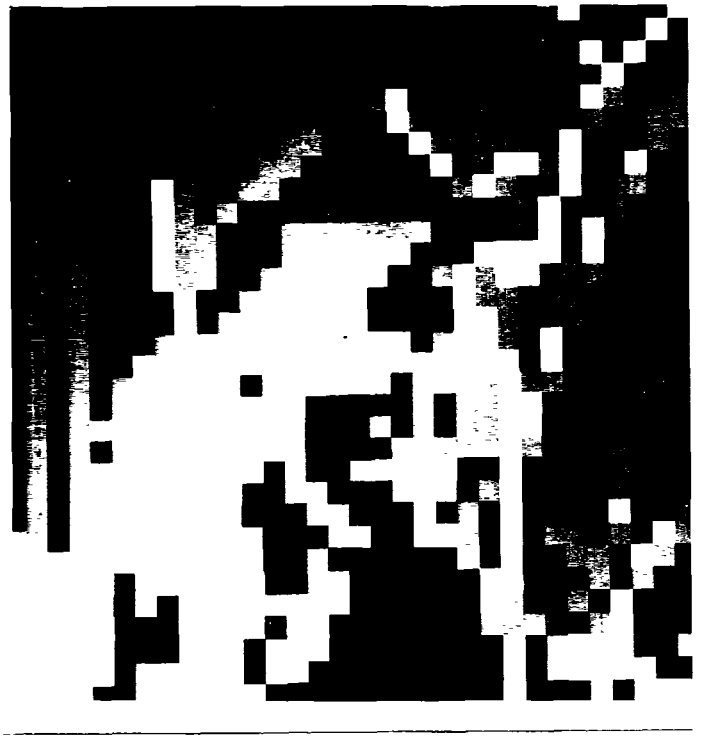

Figure 3.2: ENSD Classification Image for the 512×512 LENNA.

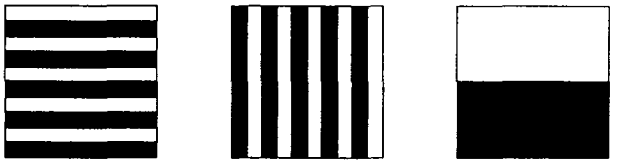

Figure 3.3: Sample Blocks.

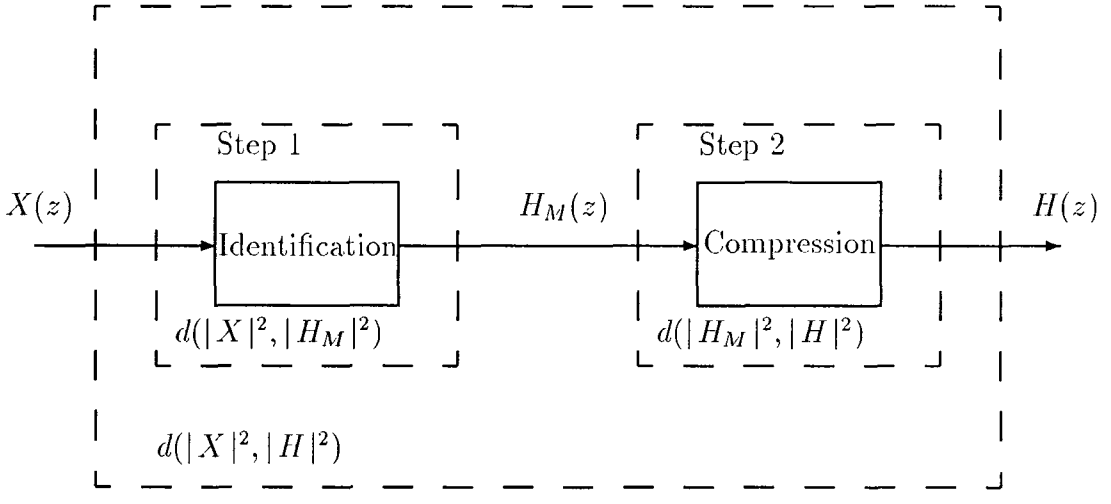

Figure 3.4: LPC Analysis as a Two-step Process.

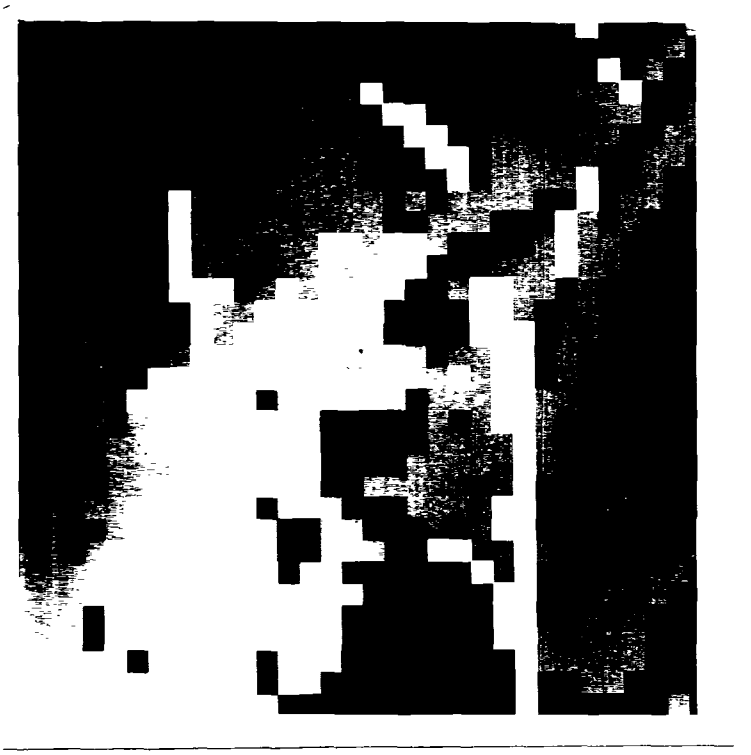

Figure 3.5: Spectral Classification Image for the 512×512 LENNA.

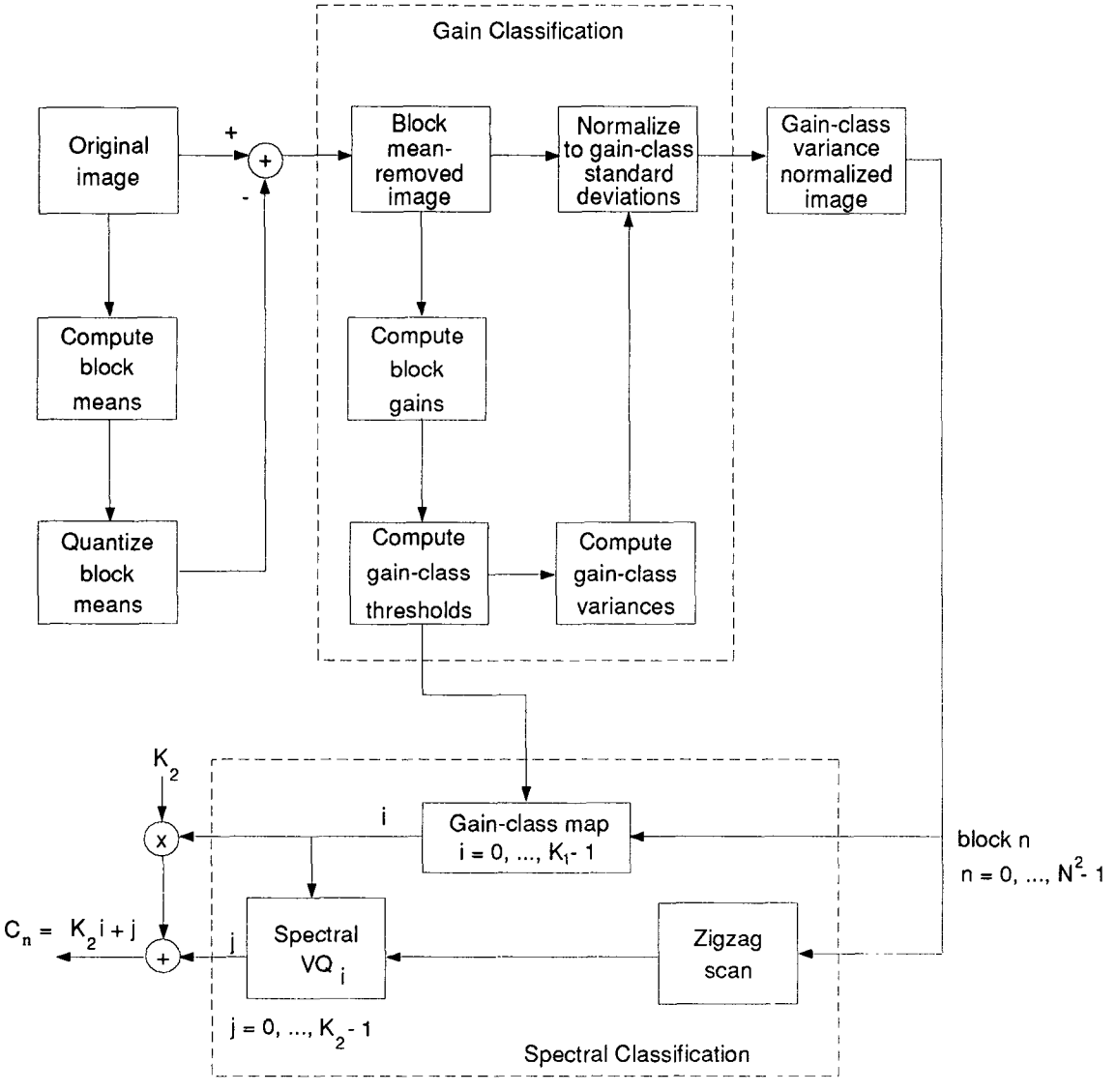

Figure 3.6: Gain-Spectral Classification Block Diagram.

Chapter 4

Image Coding Using Adaptive Discrete Cosine Transform

A 1-D signal can be represented by an orthogonal series of basis functions. Using the same idea, an image can be expanded in terms of a discrete set of basis arrays called basis images. These basis images form a vector space and can be generated by unitary matrices [Jai86].

Unitary transforms have nice properties that make them suitable for coding applications. A unitary transform is invertible and preserves the signal energy. Most unitary transforms pack a large fraction of the average energy of the signal into a few components of the transform coefficients. Since the total energy is preserved, some of the coefficients will contain very little energy and their contribution in reconstructing the original image is less than the contribution of other coefficients. The transform coefficients are almost uncorrelated and thus can be encoded efficiently using quantizers designed for memoryless sources [Jai86].

It is a well-known result that the Karhunen-Loeve transform (KLT) coefficients are uncorrelated. Also, the KLT is known to be optimal (from the energy-packing point of view [Jai86]). These properties are desirable in data compression applications. The KLT has some shortcomings which make it impractical. Especially, it depends on the statistics as well as the size of the image. Therefore, in general, its basis vectors must be computed for each image and are not known analytically. Also, a fast algorithm for the KLT is not available and therefore the number of operations for performing the transformation are quite large for images.

The Discrete Cosine Transform (DCT) is a unitary transform which is very close to the KLT of a first-order stationary Markov sequence when the correlation parameter (ρ) is close to 1 [Jai86]. This property together with the availability of a fast DCT algorithm make the DCT a good alternative for practical image coding systems. The 1-D DCT of a sequence $\{u(n),\ 0 \leq n \leq N-1\}$ is defined as

$$v(k) = c(k) \sum_{n=0}^{N-1} u(n) \cos \frac{\pi(2n+1)k}{2N}, \quad 0 \leq k \leq N-1. \tag{4.1}$$

where

$$c(0) = \sqrt{\frac{1}{N}}, \quad c(k) = \sqrt{\frac{2}{N}} \text{ for } 1 \leq k \leq N-1. \tag{4.2}$$

The only basis vector with nonzero mean is the first one and the corresponding coefficient is called the DC coefficient. The inverse transformation is given by

$$u(n) = \sum_{k=0}^{N-1} c(k)v(k) \cos \frac{\pi(2n+1)k}{2N}, \quad 0 \leq n \leq N-1. \tag{4.3}$$

Using fast algorithms, the DCT can be computed in $O(N \log N)$ operations [Jai86].

2-D DCT can be achieved by a separable 1-D DCT in the horizontal and

vertical directions. The complexity of DCT increases with increasing the size of the image. To reduce the complexity, an $N \times N$ image can be segmented into $L \times L$ blocks and then 2-D DCT is used for each block. Not only does this segmentation reduce the complexity, but also it gives the opportunity to allocate bits nonuniformly among the different activity regions of the image.

An adaptive DCT (ADCT) coding system segments the image into $L \times L$ blocks and separately encodes each block. In this manner, blocks can be encoded with different rates corresponding to the spatial activity of each block as well as different quantizers corresponding to the statistics of each block. The nonstationarity among the blocks leads us to use classification to separate the image into more homogeneous clusters. Each class contains blocks with close levels of activity if classification is only based on the activity of blocks. This can be achieved using classification schemes in Chapter 3. The variance of coefficients for each class is computed and the required bit rate for each coefficient in each class is defined using an optimal bit allocation procedure [Sho88]. After subtracting the mean of the DC coefficient, all coefficients are divided by their standard deviations (the mean of other coefficients are assumed to be zero).

The normalized coefficients are quantized using scalar quantizers. The quantization scheme used in this work is a modified version [Lee93] of the entropy-constrained trellis-coded quantizer (ECTCQ) first reported in [Fis92]. The ECTCQ exploits the space-filling efficiency of the trellis codes and can realize a significant portion of the so-called *space-filling advantage* [Loo89]. The ECTCQ has been demonstrated to provide an excellent rate-distortion performance for a large variety of memoryless sources. The ECTCQ proposed in [Lee93] places a symmetry constraint upon the reproduction codebook. This symmetry con-

straint, while essentially costing no performance loss, can be used to reduce the memory requirement in entropy coding of the ECTCQ output. The quantizers are designed for the so-called Generalized Gaussian Distributions (GGD) [Far84]. The probability density function associated with the GGD is given by:

$$p(x) = [\frac{\alpha\eta(\alpha,\beta)}{2\Gamma(1/\alpha)}] \exp(-[\eta(\alpha,\beta) \mid x \mid]^{\alpha}), \tag{4.4}$$

where

$$\eta(\alpha,\beta) = \beta^{-1}[\frac{\Gamma(3/\alpha)}{(1/\alpha)}]^{1/2}, \tag{4.5}$$

and $\alpha > 0$ is a shape parameter describing the exponential rate of decay, β is the standard deviation of the distribution and $\Gamma(.)$ is the gamma function. The shape parameter α can be determined from a test sequence obtained from typical images using the Kolmogorov-Smirnov test [Con71].

The classification table, the variances, the mean of the DC coefficients and the design rate are sent to the receiver as side information. The mean of the other coefficients are assumed to be zero. The assigned bit rate for some coefficients might be zero in which case their variance will not be transmitted. The allocated bit rates can be found at the receiver using the same bit allocation procedure. A more efficient way to transmit the side information can be found in [Ran92].

4.1 Bit Allocation

The problem of bit allocation is that of optimally distributing available bits among the different quantizers in a coding system. The objective of bit allocation is to achieve the smallest possible average distortion. Each quantizer is capable of operating at one of a fixed number of rates. The performance of such a

quantizer is characterized by its quantizer function (QF), defined by the average quantization distortion as a function of the rate [Ber71].

Suppose we have M sequences of data samples to encode and r_i, the average rate for coding the i^{th} sequence, can be chosen from a discrete set of available rates. For the above ADCT scheme, there are $M = L^2C$ sequences where C is the number of classes. Defining $\hat{X}$ as the reconstructed version of the encoded X in the i^{th} sequence, $D_i(r_i) = E_i[(X - \hat{X})^2]$ is the mean square error for coding the i^{th} sequence as a function of the rate where E_i is the expectation in the i^{th} sequence. It is a well-known fact that [Ber71]

$$D_i(r_i) = \sigma_i^2 d_i(r_i) \tag{4.6}$$

where σ_i^2 and $d_i(r_i)$ are the variance and the QF of the i^{th} sequence respectively. If P_i is defined as the probability of having a block in class i, the problem is that of determining

$$\min_{r_i} \; D = \sum_{i=1}^{M} P_i \sigma_i^2 d_i(r_i), \tag{4.7a}$$

$$\text{subject to} \sum_{i=1}^{M} P_i r_i = R. \tag{4.7b}$$

In practice, P_i and σ_i^2 are computed empirically from the data.

There are different methods to solve the problem [Tru81], [Sho88], [Ris91]. When all QF's are convex and nonincreasing, which is the case for our quantizers, the following simple Steepest-Descent algorithm is optimal:

1. Set $r_i = 0.0$ for $i = 1, 2, \ldots, M$.

2. Compute the index i' which satisfies

$$i' = \mathbf{arg} \max_{1 \le i \le M} \{\sigma_i^2 \frac{d_i(r_i) - d_i(r_i + \Delta r_i)}{\Delta r_i}\},$$

where Δr_i is the difference between r_i and the next available rate for the i^{th} sequence.

3. Set $r_{i'} = r_{i'} + \Delta r_{i'}$.

4. If $R \geq \sum_{i=1}^{M} P_i r_i$, stop; otherwise go to 2.

4.2 Comparing Adaptation Schemes

Any of the classification schemes we developed in Chapter 3 can be used for 2-D ADCT coding of images. The sequence of DC coefficients is modeled by a Gaussian distribution and all other sequences are modeled by a generalized Gaussian distribution with parameter 0.6. The simulation results for the 512×512 monochrome Lenna image is shown in Figure 4.1. For an $M \times N$ image, the peak signal-to-noise ratio (PSNR) is defined by

$$PSNR = 10 \log_{10} \frac{(255)^2}{\frac{1}{MN} \sum_{i=1}^{M} \sum_{j=1}^{N} (x_{ij} - \hat{x}_{ij})^2}, \tag{4.8}$$

where x_{ij} and $\hat{x}_{ij}$ are the pixels of original and reconstructed images respectively. The encoding rates in these results include all required bits for transmitting the side information as overhead. The variance of coefficients and the mean of the DC coefficients are assumed to be quantized with high precision (using 8-bit scalar quantizers). The classification table and the design rate are sent losslessly. In the process of bit allocation, some of the coefficients are assigned zero bits. To avoid sending the variance of these coefficients which are not needed at the receiver and can be considered as zero, first we zigzag scan the allocated bits. Starting from the last allocated bit (which is usually zero) we go through the list until we find a nonzero variance. The location of the first nonzero element

and all variances after that are transmitted to the receiver. We repeat the same procedure for all classes. Using this simple algorithm, we save about 50 percent in overhead for rate $r = 0.25$ bits/pixel. Another useful idea for reducing the overhead is suggested in [Ran92] which works both for high and low rates. Saving in overhead is a general reduction for all schemes in Figure 4.1 and will not change the comparison. Using the spectral classification improves the results by about 0.7 dB for rate $r = 0.25$ bits/pixel and a block size of 16. The results based on the spectral classification are better than the results based on the other classification schemes; however, the results for gain-based classifications are more-or-less the same. The perceptual comparison of the results shows that the ENSD classification outperforms the Chen-Smith classification. We have conducted informal subjective tests in Communications and Signal Processing Laboratory on the relative performances of the three different techniques that we have considered. We asked students to compare the reconstructed images for the 512×512 Lenna for a rate of 0.25 bits/pixel (Fig. 4.1). Among 50 students who were asked, 43 of them preferred the spectral classification over the gain-based classifications. Also, 46 students liked the ENSD classification result better than the Chen-Smith classification result.

Table 4.1 shows the effects of block size on the PSNR. Best performance is achieved by using a block size of 16. Reconstructed images for rate=0.25 bits/pixel are presented in Figure 4.2.

Another important issue is the effect of quantizers on the performance of the system. Using quantizers designed for the Laplacian distribution for the non-adaptive system degrades the result by about 0.5 dB for rate r=0.25 bits/pixel. On the other hand, our primary results show that the effect of changing quan-

Design Rate = 0.25 Bits/Pixel				
	Nonadaptive		Spectral	
Block Size	Operating Rate	PSNR(dB)	Operating Rate	PSNR(dB)
8	0.244	31.79	0.262	32.61
16	0.239	32.69	0.246	33.47
	Chen-Smith		ENSD	
Block Size	Operating Rate	PSNR(dB)	Operating Rate	PSNR(dB)
4	0.248	24.08	0.247	24.11
8	0.261	32.53	0.266	32.65
16	0.253	33.42	0.251	33.39
32	0.251	32.70	0.251	32.73

Table 4.1: ADCT Simulation Results for the 512×512 LENNA.

tizers for the ADCT system is negligible. As a result, the difference between the performance of the nonadaptive system and the adaptive systems in Figure 4.1 will increase by using Laplacian quantizers. The simulation results indicate that the ADCT system is more robust with respect to the choice of quantizers.

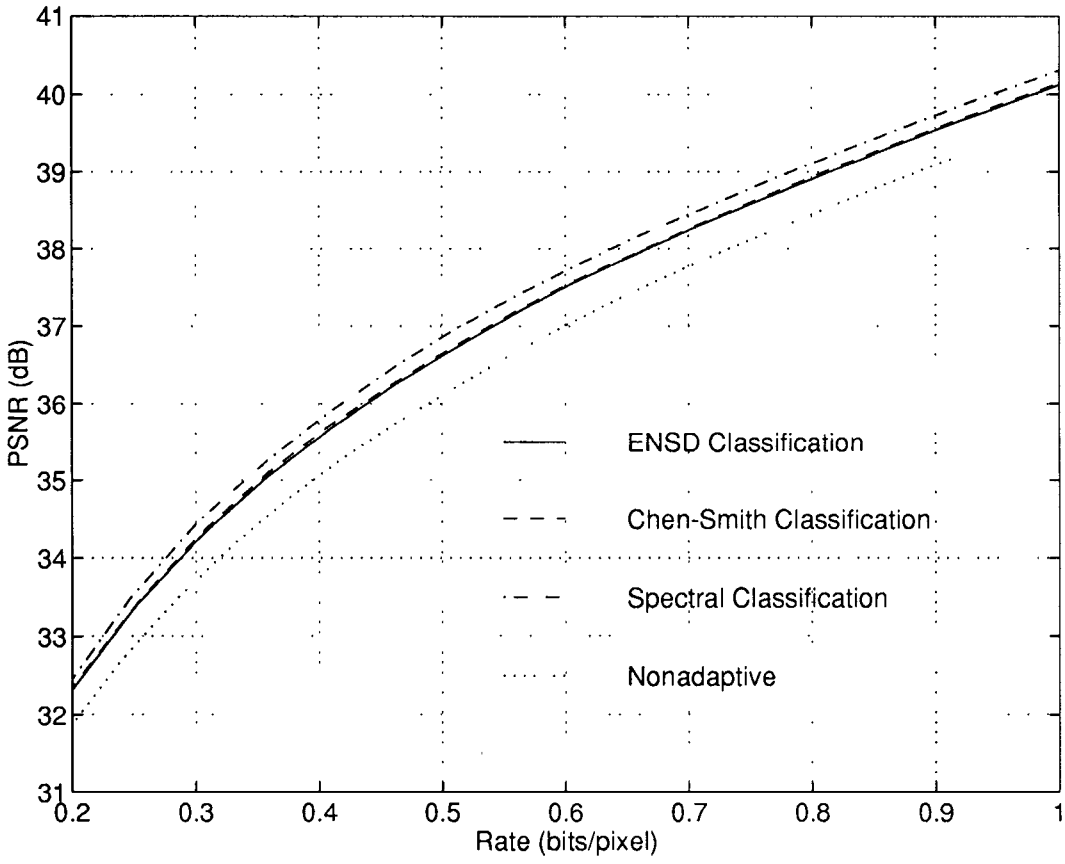

Figure 4.1: ADCT Simulation Results for the 512×512 LENNA (block size = 16).

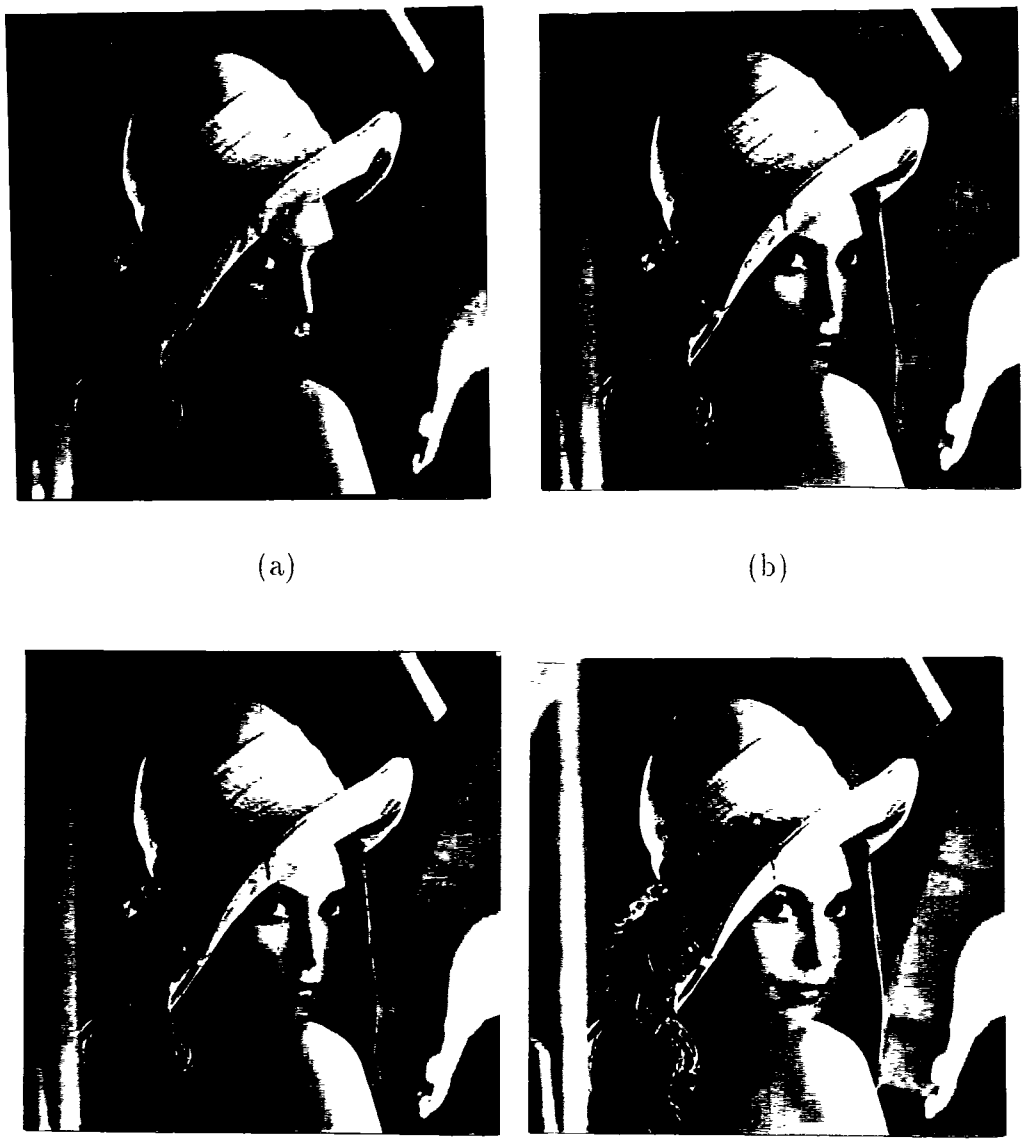

(a) (b)

(c) (d)

Figure 4.2: Reconstructed Images for the 512 × 512 LENNA (Rate = 0.25 Bits/Pixel): (a)Nonadaptive, (b)Spectral Classification, (c)Chen-Smith Classification and (d)ENSD Classification.

Chapter 5

Wavelet Coding of Images

Image coding based on subband or discrete wavelet transform (DWT) ideas has received much attention in recent years [Woo86], [Mal89], [Ant92]. Not only do these coding techniques provide good compression results (in a rate-distortion sense), but also they are suitable for progressive transmission and provide a multi-resolution capability – a feature that is becoming increasingly important for the seamless communication networks of the future. As discussed in Chapter 2, the basic idea behind the DWT is to decompose the input signal into two components: (i) a *low-resolution approximation* and (ii) a *detail signal.* This results in a decomposition of the input signal into two components which can be considered as low-pass and high-pass versions of the original signal, generally referred to as subbands. Each of the resulting subbands can be further decomposed using the same approach. In this manner, the DWT decomposes a given input signal into a number of frequency bands.

The DWT can be easily implemented using linear phase finite impulse response filter banks [Ant92]. Two-dimensional (2-D) extensions of the DWT can be obtained by a separable decomposition in the horizontal and vertical direc-

tions [Woo86], [Mal89]. Using a 2-D separable DWT based on the No. 2 7-9 spline filters in [Ant92], an image is decomposed into 16 subbands. The statistics of the subbands for the 512×512 Lenna is given in Table 5.1.

The statistical properties of the low frequency subband (LFS) are similar to those of the original image and therefore well-established techniques for image compression such as 2-D DPCM and transform coding are suitable for encoding the LFS [Tan92]. Furthermore, the LFS exhibits a nonstationary behavior, as in the original image, and some type of nonuniform bit allocation among the different activity regions of the LFS should be useful. It is also observed in [Tan92] that all other subbands, hereafter referred to as high frequency subbands (HFS's), have small intraband correlation coefficients and thus can be encoded efficiently using quantizers designed for memoryless sources. However, a simple inspection of the 16 subbands reveals that in fact the bulk of the energy in the 15 HFS's is concentrated more-or-less in the vicinity of areas which correspond to edge activity in the original image. A similar observation on the dependency of HFS's is also made in [Nav93]. This implies that those areas of the HFS's that contain most of the information must be encoded more finely than the rest. Not only is this classification important from a rate-distortion point of view, but also it perceptually improves the quality of the encoded image.

The above two observations constitute the motivation for the coding system developed in this chapter. Here, we concentrate on the problem of classifying the blocks of the different subbands (the LFS and a set of the HFS's) into a number of classes and using an appropriate bit allocation scheme [Woo92] followed by quantization to efficiently encode the subbands. The classification schemes used here are those designed in Chapter 3. The block diagram of the proposed system

is illustrated in Figure 5.1.

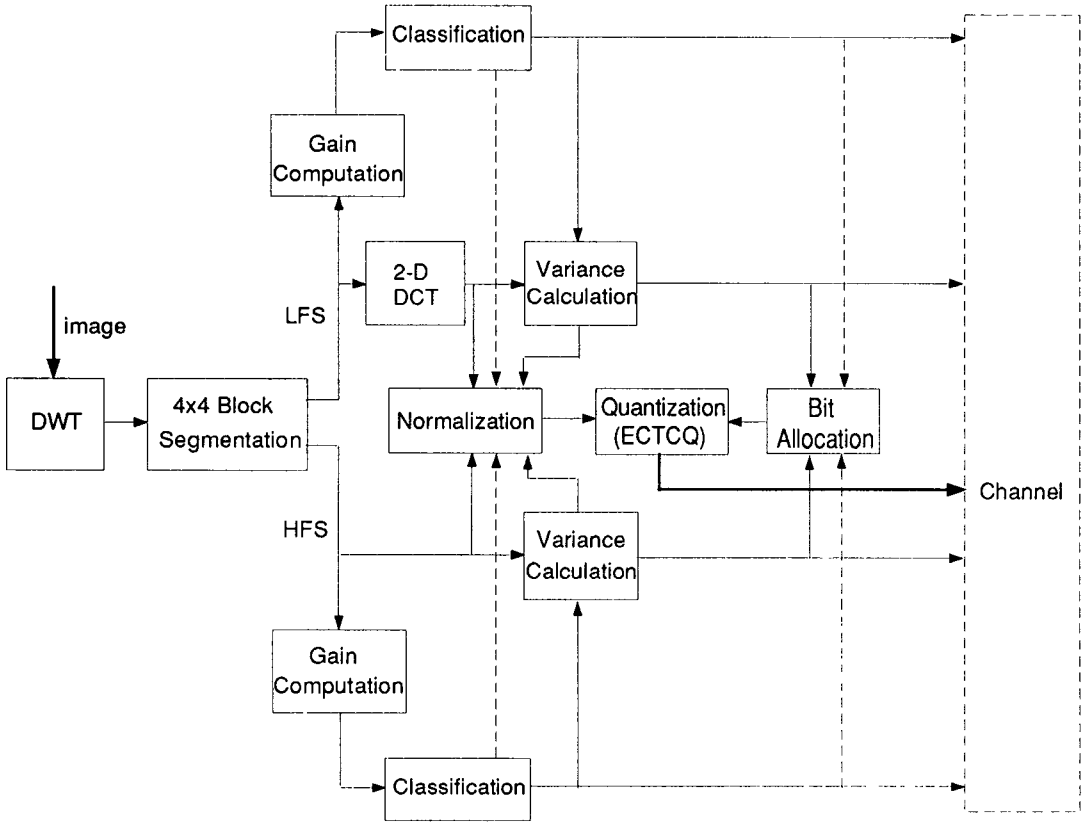

Figure 5.1: System Block Diagram.

5.1 Quantization of Low Frequency Subbands

The similarity between statistical properties of the LFS and the original image suggests using a conventional image coding technique for the LFS. Therefore, we use the ADCT schemes developed in Chapter 4 to encode the LFS (Fig. 5.1). The LFS is a low-resolution version of the original image and therefore it is not needed to use large block sizes. On the other hand, using smaller block

sizes reduces the complexity of the DCT computations. In this work, the block size is 4×4 and the LFS blocks are split into one of four classes unless stated otherwise. The same quantizers as those used in Chapter 4 are used for the DCT coefficients of the LFS. However, bits are allocated to all subbands together using the procedure described in Section 4.1.

5.2 Quantization of High Frequency Subbands

High- and low-energy portions of HFS's are separated into two energy classes. Clearly, the higher is the variance of a subband, the more significant will be its influence on the final results. Table 5.1 shows that most of HFS's have very low variances and will not need high bit rates. Because classifying a subband costs an overhead for the transmission of the corresponding classification table, it would be inefficient to classify all HFS's. Therefore, we usually perform the classification only on the four HFS's with highest variances. As an alternative, to reduce the complexity of the system and the overhead due to the classification tables, we may only classify the HFS with the highest variance and use its classification table for encoding the other subbands. This will not degrade the overall performance of the system too much because as can be seen in Figure 5.2, the high-energy portion of different subbands are almost located in the same area and the saving in the overhead will compensate for the inaccuracies of the classification tables. Also, different combinations of the classification tables can be used to reduce the overhead. This issue is discussed in the following sections.

5.3 System Overhead

To reconstruct a replica of the original image at the receiver, in addition to quantized samples of the decomposed image, some overhead information also need to be transmitted. Specifically, the overhead includes: the classification table of each subband, the variance of each sequence, the design rate and the mean of the DC coefficients of the LFS. The allocated rate for each sequence can be recomputed when the design rate, the variances and the number of coefficients in each class are known by performing the bit allocation procedure at the receiver. Therefore, instead of transmitting the allocated rates, the design rate is sent to the receiver. The knowledge of the variances and the mean of the DC coefficients is crucial in the process of renormalizing the quantized samples. They are transmitted with small distortion using 8-bit quantizers.

The classification tables constitute a significant portion of the overhead. There are 1024 blocks of 4×4 samples in each of the 16 subbands of a 512×512 image. Using four classes for the LFS, 2048 bits or 0.0078 bits/pixel is needed to be transmitted for the classification table of the LFS. HFS's are split into two classes and the classification of each HFS costs 0.0039 bits/pixel. The overhead is a significant portion of the bit rate for low rates. For example, when four HFS's are classified, for an encoding rate of 0.25 bits/pixel, more than 10 percent of the bit rate is used to send the side information.

Figure 5.2 shows that the high-energy portion of different subbands are almost located in the same area. To reduce the complexity of the system and the overhead due to the classification tables, we have only classified the HFS with the highest variance and use its classification table for the other three classes. This will not degrade the overall performance of the system too much and the

saving in the overhead will compensate for the inaccuracies of the classification tables. Also, different combinations of the classification tables can be used to reduce the overhead. For example, the two HFS's with highest variances can be classified separately and a combination of the resulting classification tables used for all subbands. The relative merits of these different alternatives are carefully investigated and will be reported in the following section.

Another way to reduce the overhead is by using lossless coding schemes for transmitting the classification tables. We have used adaptive Huffman coding to compress the classification tables.

5.4 Simulation Results and Comparison

To compare the different classification strategies in a meaningful way, the quantizers that have been used in the system are fixed. Let us stick with an ECTCQ designed for the GGD with $\alpha = 0.6$ for all sequences except the DC coefficients of the DCT in which an ECTCQ designed for the Gaussian distribution is used. We have used arithmetic coding for ECTCQ's to achieve a rate closed to the ECTCQ output entropy. In what follows we consider a number of different configurations. The base system considered includes the classification of the LFS into four classes and the classification of four HFS's with highest variances into two classes (System A). System A is used to compare the Chen-Smith and the equal-normalized-standard deviation classifications in Table 5.2 and Figure 5.3. It is clear that the results using the Chen-Smith classification are about 0.3 dB inferior for low bit rates. This is because the high-energy part of each subband usually consists of about 20 percent of the blocks instead of 50 percent assumed

by the Chen-Smith algorithm (Fig. 2.5). In fact, our experiments indicate that at low rates (less than 0.35 bits/pixel for Lenna) the optimal bit allocation procedure only assigns nonzero bit rates to the high-energy classes of the HFS's. This implies that for this range of rates, only a small portion of each subband is important enough to be encoded and using an equi-populous classification scheme will (i) waste the available bits to code less important parts and (ii) not allocate enough bits to the important portions.

Now, using the equal-normalized-standard deviation criterion, we study the tradeoff between classifying more subbands and saving in overhead. The following systems which all use four classes for the LFS are considered:

- System A: Classify four HFS's with highest variances.
- System B: Classify the HFS with highest variance and use its classification table for the four subbands with highest variances.
- System C: Classify the two HFS's with highest variances. Construct a classification table which is the logical OR of the classification tables and use it for the four subbands.
- System D: The same as System B except using the classification table for all subbands.
- System E: The same as System C except using the classification table for all subbands.
- System F: The system without any classification.
- System G: The system with classification only for the LFS.

Figure 5.4 compares the simulation results of Systems A, B and F for the 512×512 Lenna. It is clear that classification improves the performance by about 0.7 dB for a rate of 0.25 bits/pixel. System A outperforms System B for a large range of rates. This improvement is achieved because the HFS's are classified more accurately in System A. On the other hand, System B outperforms System A for very low bit rates. Here, the reduced overhead due to the classification tables in System B compensates for the degraded classification.

The two HFS's with highest variances are usually the HFS's neighboring the LFS (Table 5.1). Table 5.1 shows that Subbands 2 and 5 have large column and row correlations respectively. There is a dependency between Subband 2 and Subbands 3, 4, 7 and 8 which all have large column correlations [Nav93]. Also, Subband 5 and Subbands 9, A, D and E are dependent and their row correlations are large. Therefore, it is more reasonable to use Subbands 2 and 5 to construct a unique classification table than to use one of them as the classification table. Figures 5.5 and 5.7 confirm the above fact.

Figure 5.6 shows that using the adaptation for all HFS's improves the performance of the system for high rates. At low rates the optimal bit allocation procedure assigns zero (or very low) bit rates to the HFS's with low variances. Therefore, the effect of these subbands in the final result is not important.

Figure 5.9 shows the effects of classifying the LFS alone. For a bit rate of 0.25 bits/pixel, using adaptation for the LFS improves the performance by about 0.2 dB.

System E is our best system in the sense that not only does it achieve the best peak signal-to-noise ratio, but also its complexity is less than System A and comparable with other systems. In Figure 5.10 we compare our results for the

512×512 monochrome Lenna image with, to our knowledge, some of the best results reported in the literature [Tan92], [Nav93], [Kim92], [Sha93]. Clearly our proposed System E exhibits a superior rate-distortion performance. We must mention that our System F is essentially the same as the system described in [Sri92] with the exception of the ECTCQ's which are designed based on a training sequence approach in [Sri92]. The results in [Sri92] are about 0.5 dB better than our results for System F. At this point, we can attribute this difference only to the different quantizers. Although we have not tried it, it is conceivable that a training sequence approach for the quantizer design can lead to similar improvements for other mentioned systems. In other words, using the adaptation described here may improve the results in [Sri92] as well.

Subband	Mean	Variance	Row Correlation	Column Correlation
Image	124.05	2290	0.971	0.985
1	124.00	2153	0.881	0.948
2	0.004	10.63	-0.128	-0.424
3	-0.004	0.70	0.010	-0.208
4	0.008	1.50	-0.100	0.223
5	-0.031	27.67	-0.292	0.197
6	0.019	7.24	-0.071	-0.242
7	0.004	0.68	0.145	-0.260
8	0.001	1.63	0.071	0.249
9	-0.023	1.99	-0.337	0.121
A	0.010	1.124	-0.256	0.006
B	0.003	0.464	-0.131	-0.151
C	-0.002	0.53	-0.150	0.064
D	-0.005	5.71	0.209	0.128
E	-0.024	2.26	0.235	-0.090
F	-0.002	0.47	0.056	-0.181
G	-0.006	0.80	0.145	0.219

Table 5.1: Statistics of 16 Subbands of the 512×512 LENNA.

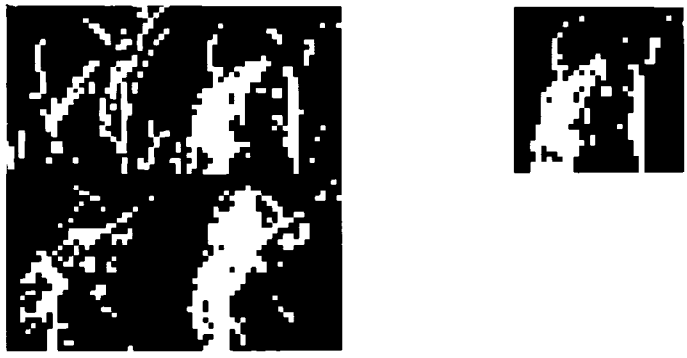

Figure 5.2: Classification Image for the 512×512 LENNA Subbands.

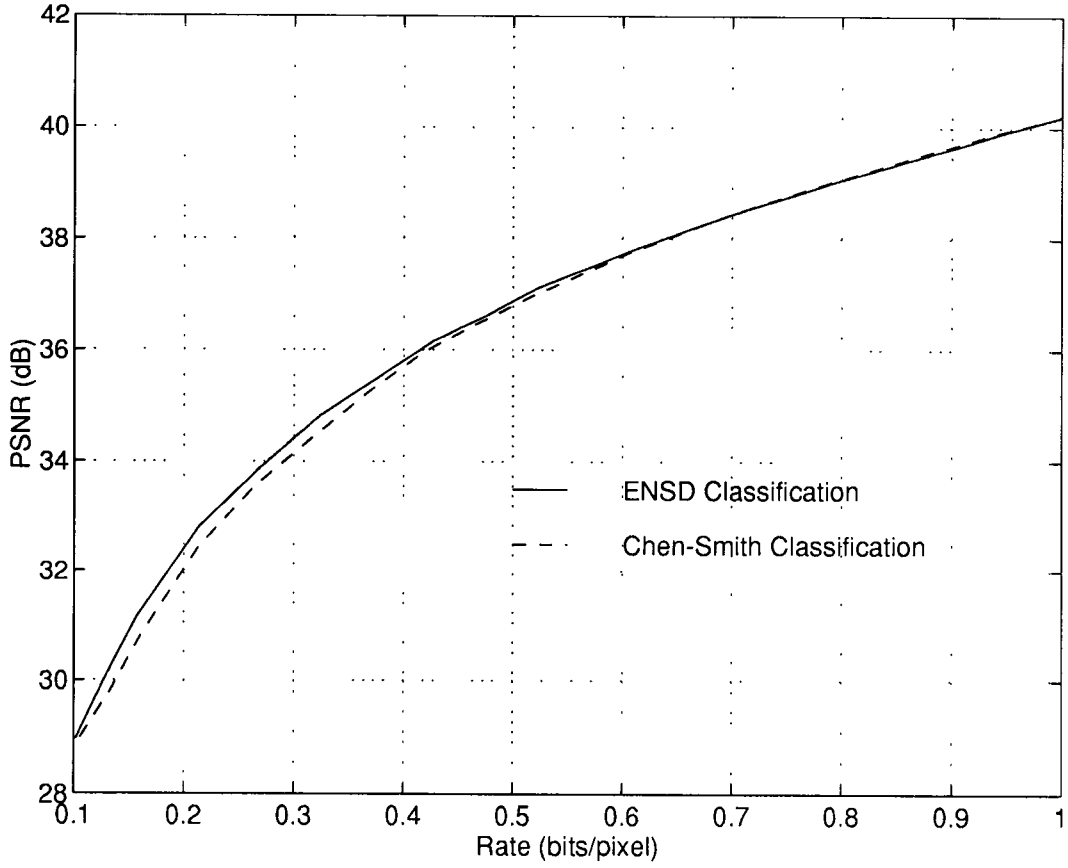

Figure 5.3: Comparing Different Classification Schemes for the 512×512 LENNA.

	Chen-Smith		ENSD	
Design Rate	Operating Rate	PSNR(dB)	Operating Rate	PSNR(dB)
0.25	0.268	33.57	0.268	33.87
0.50	0.518	36.98	0.523	37.13
0.75	0.734	38.67	0.743	38.72

Table 5.2: Simulation Results of Different Classification Schemes for the 512×512 LENNA.

Design Rate = 0.25 Bits/Pixel				
	Chen-Smith		ENSD	
Block Size	Operating Rate	PSNR(dB)	Operating Rate	PSNR(dB)
2	0.250	31.09	0.232	31.70
4	0.268	33.57	0.268	33.87
8	0.263	33.65	0.265	33.74

Table 5.3: Comparing Different Block Sizes for the 512×512 LENNA.

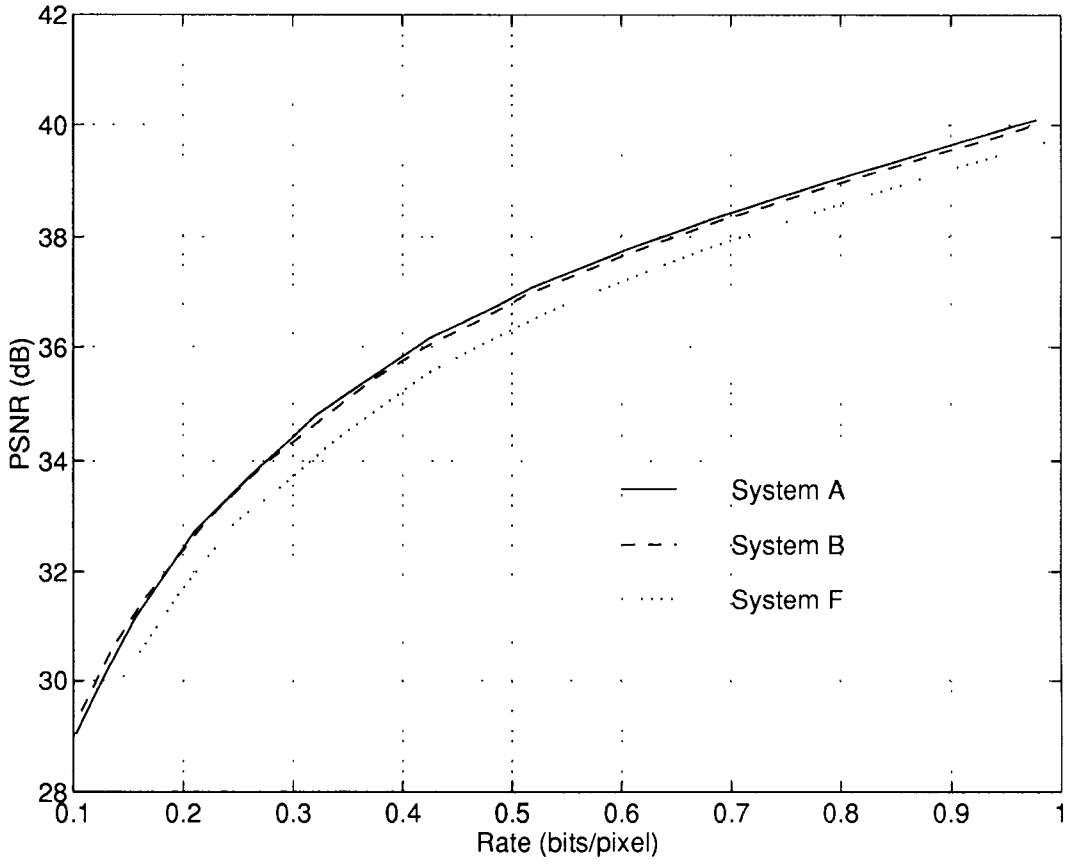

Figure 5.4: Comparing Systems A, B and F for the 512×512 LENNA.

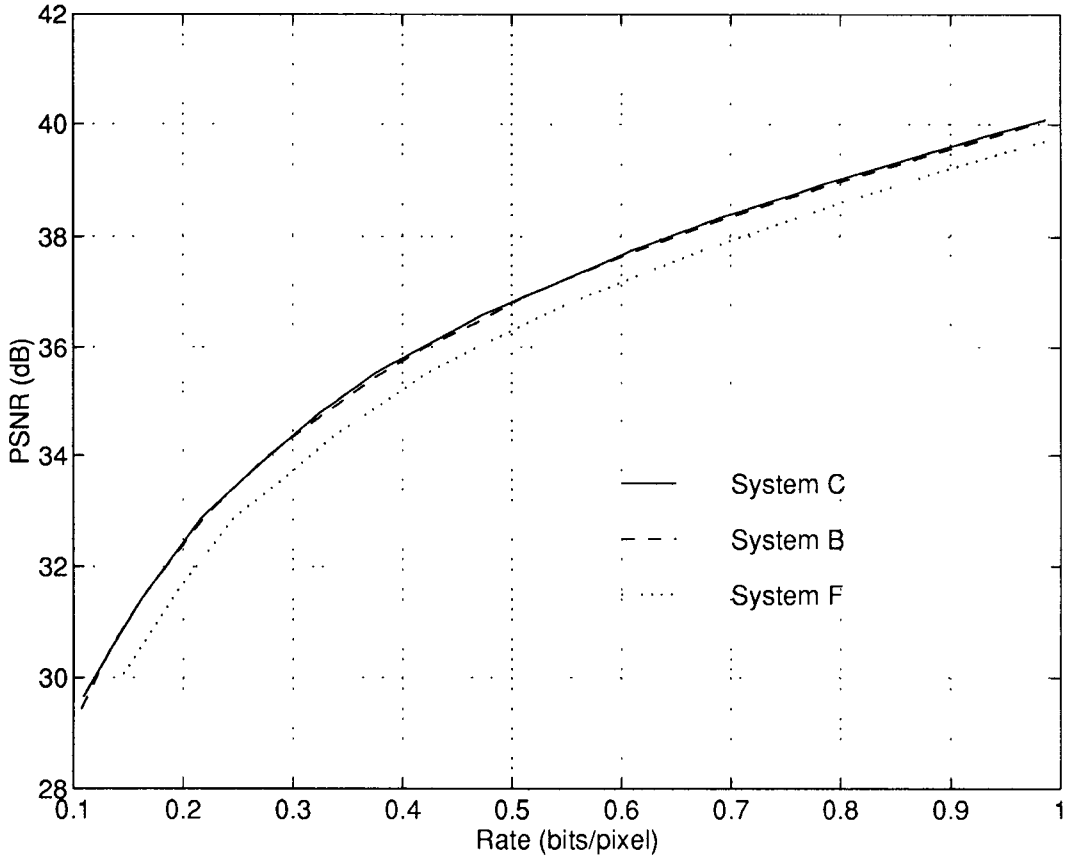

Figure 5.5: Comparing Systems B, C and F for the 512×512 LENNA.

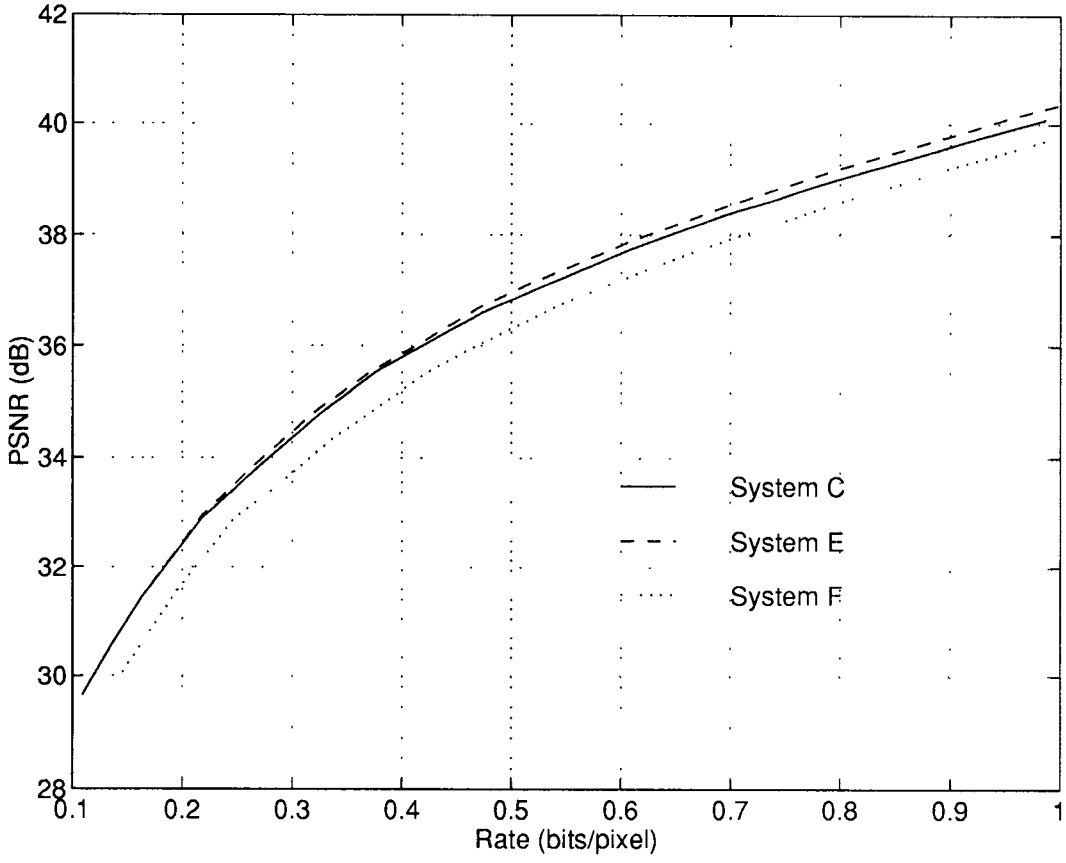

Figure 5.6: Comparing Systems C, E and F for the 512×512 LENNA.

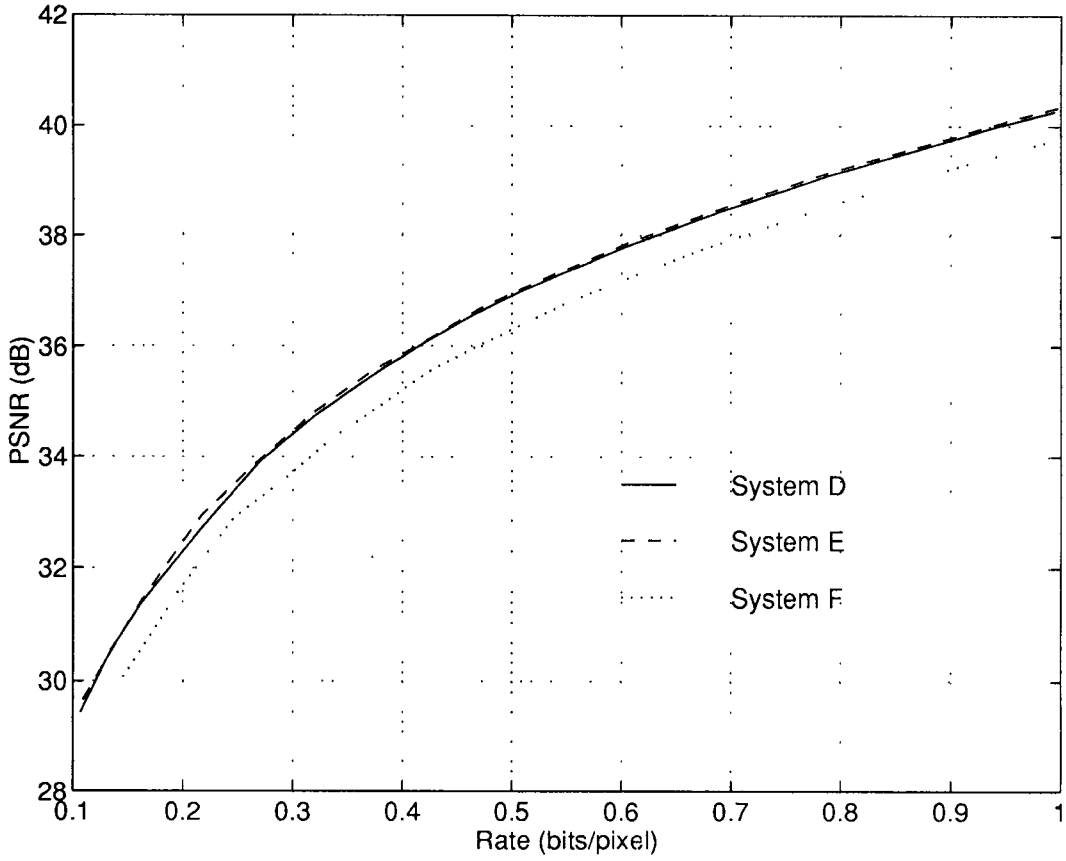

Figure 5.7: Comparing Systems D, E and F for the 512×512 LENNA.

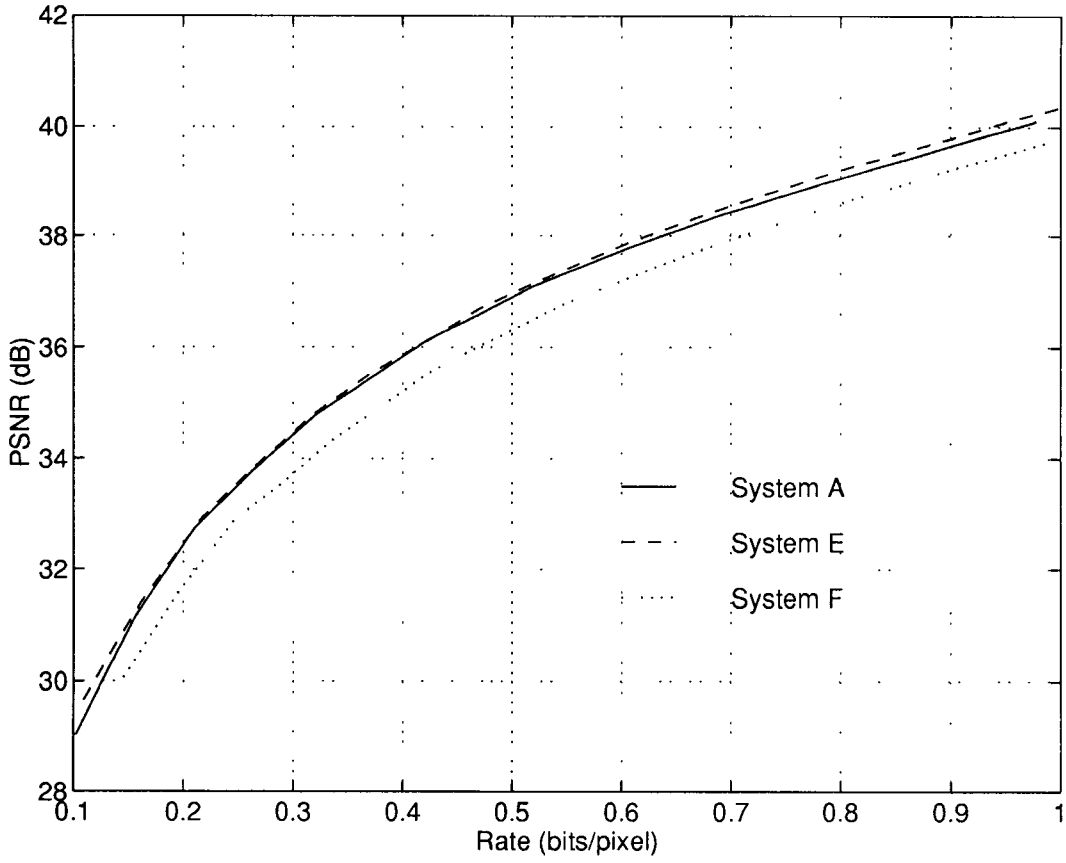

Figure 5.8: Comparing Systems A, E and F for the 512×512 LENNA.

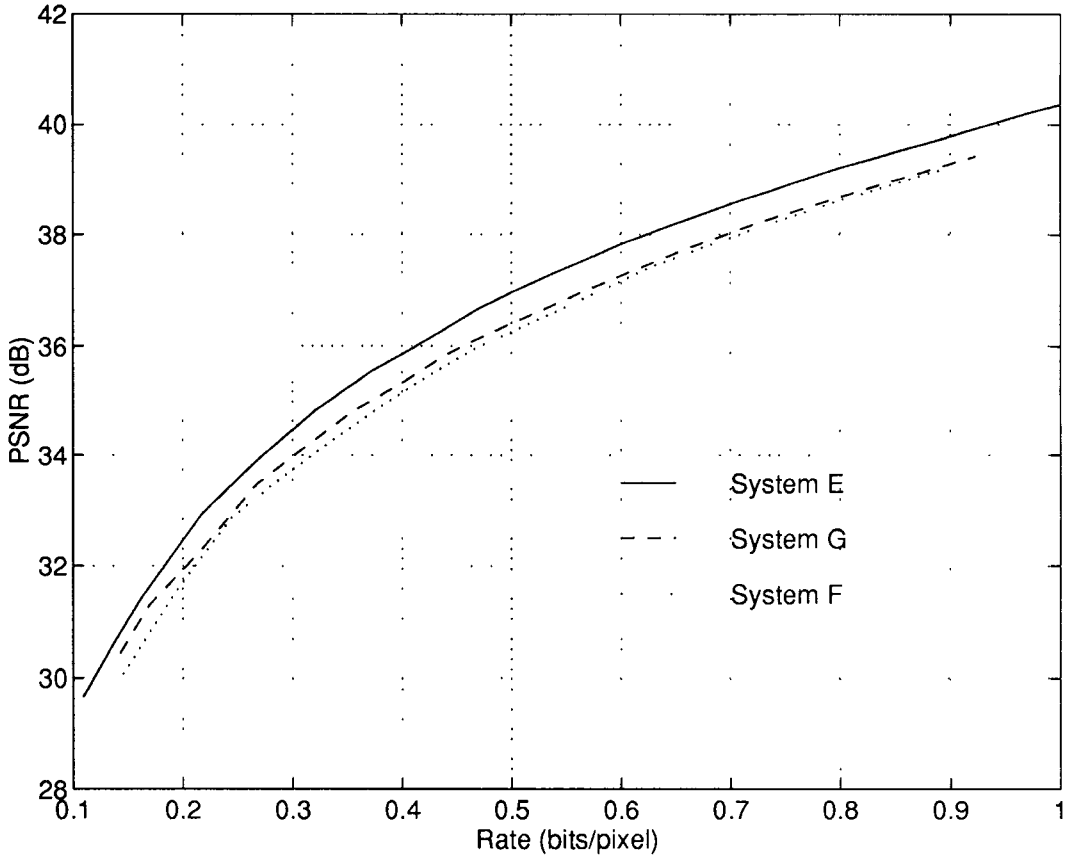

Figure 5.9: Comparing Systems E, F and G for the 512×512 LENNA.

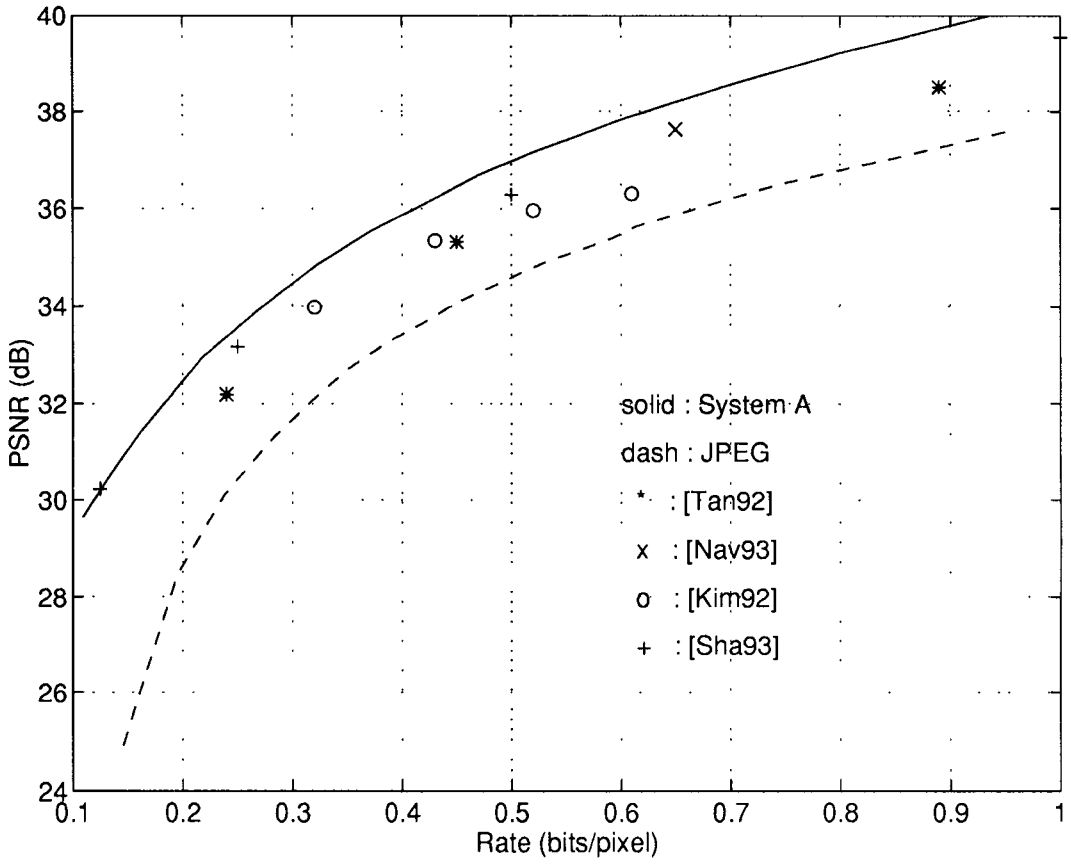

Figure 5.10: Performance of Different Image Coding Systems for the 512×512 LENNA.

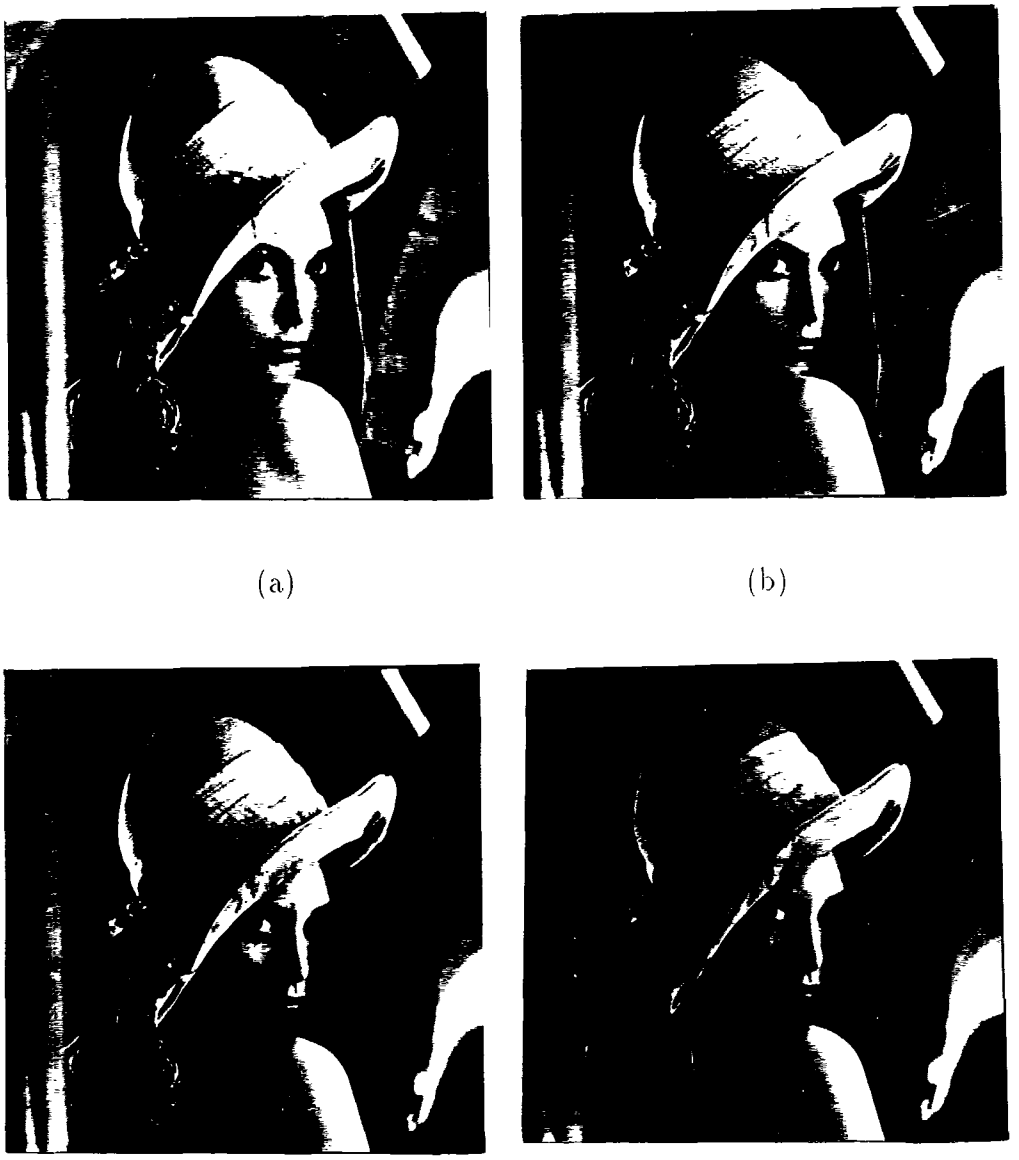

(a) (b)

(c) (d)

Figure 5.11: Reconstructed Images for System A (all rates in Bits/Pixel): (a)Rate = 0.25, (b)Rate = 0.5, (c)Rate = 0.75 and (d)Rate = 1.0.

Chapter 6

Conclusion

We now present a summary of image coding systems we developed in this thesis and comment on the performance of these systems. We finish this chapter by giving some ideas for future work.

In Chapter 3, we developed two new classification schemes and the results of Chapter 4 shows that both of them outperform the well-known Chen-Smith classification scheme for an ADCT image coding system. Also, the results in Chapter 5 show that using the ENSD classification scheme for our new proposed image coding system has some advantages over using the Chen-Smith classification scheme.

A new method to combine classification and bit allocation was introduced in Section 3.2. An algorithm to solve the problem was given although the implementation of this algorithm is left as a future work.

In Chapter 5, we developed a new adaptive wavelet based image coding system. Simulation results show that the proposed system exhibits a superior rate-distortion performance over, to the best of our knowledge, all wavelet based image coding systems reported in the literatures. Different versions of the proposed

system are considered and a discussion of the tradeoff between the complexity and the performance of the systems is given in Chapter 5.

One of the classification schemes we developed is the spectral classification. The proposed spectral classification scheme uses 1-D spectral characteristics of the blocks to classify them. An open problem is how to design a 2-D version of the spectral classification. Such a system should outperform the existing 1-D version of the spectral classification.

In Chapter 5, we have used ADCT to encode the LFS of the image. A block size of 4 is used and the complexity is small. However, to reduce the complexity, we are working on developing an encoder for the LFS which does not use transform coding.

Bibliography

[Ant92] Antonini M.; Barlaud M.; Mathieu P. and Daubechies I. Image Coding Using Wavelet Transform. *IEEE Trans. Image Proc.*, pages 205–220, Apr. 1992.

[Ber71] Berger T. *Rate Distortion Theory* . Prentice-Hall, 1971.

[Buz80] Buzo A.; Gray,Jr. A.H.; Gray R.M. and Markel J.D. Speech Coding Based upon Vector Quantization. *IEEE Trans. Acoust., Speech, Signal*, pages 562–574, Oct. 1980.

[Che77] Chen W.H. and Smith C.H. Adaptive Coding of Monochrome and Color Images. *IEEE Trans. on Com.*, pages 1285–1292, Nov. 1977.

[Con71] Conover, W.J. *Practical Nonparametric Statistics* . John Wiley & Sons, Inc., 1971.

[Cro76a] Crochiere R.E.; Webber S.A. and Flanagan J.L. Digital Coding for Speech in Subbands. *Bell Syst. Tech. J.*, pages 1069–1085, Oct. 1976.

[Cro76b] Croisier A.; Esteban D. and Galand C. Perfect Channel Splitting by Use of Interpolation / Decimation / Tree Decomposition Techniques. *Proc. of the Int. Conf. on Inf. Sci. and Sys.*, pages 443–446, Aug. 1976.

[Far84] Farvardin N. and Modestino J. W. Optimum Quantizer Performance for a Class of NonGaussian Memoryless Sources. *IEEE Trans. Inf. Theory*, pages 485–497, May 1984.

[Fis92] Fischer T. and Wang M. Entropy-Constrained Trellis-Coded Quantization. *IEEE Trans. Inform. Theory*, pages 415–426, Mar. 1992.

[Ger79] Gersho A. Asymptotically Optimal Block Quantization. *IEEE Trans. Inform. Theory*, pages 373–380, July 1979.

[Hay91] Haykin S. *Adaptive Filter Theory* . Prentice-Hall , 1991.

[Ita68] Itakura F. and Saito S. Analysis Synthesis Telephone Based upon the Maximum Likelihood Method . *Conf. Rec., 6th Int. Congr. Acoust.*, 1968.

[Jai86] Jain A.K. *Fundamentals Digital Image Processing* . Prentice-Hall , 1986.

[Kim92] Kim Y.H. and Modestino J.W. Adaptive Entropy Coded Subband Coding of Images. *IEEE Trans. Image Proc.*, pages 31–48, Jan. 1992.

[Lee93] Lee C.-C. and Farvardin N. Entropy-Constrained Trellis Coded Quantization: Implementation and Adaptation. *Proceedings, Conf. on Information Sciences and Systems*, pages 342–347, Mar. 1993.

[Lin80] Linde Y.; Buzo A. and Gray R.M. An Algorithm for Vector Quantizer Design . *IEEE Trans. Commun.*, pages 84–95, Jan. 1980.

[Loo89] Lookabaugh T. and Gray R. High-Resolution Quantization Theory and the Vector Quantizer Advantage. *IEEE Trans. Inform. Theory*, pages 1020–1033, Sep. 1989.

[Mal89] Mallat S.G. A Theory for Multiresolution Signal Decomposition : The Wavelet Representation. *IEEE Trans. Pattern Anal. and Mach. Intel.*, pages 674–693, Jul. 1989.

[Mar76] Markel J.D.; and Gray, Jr. A.H. *Linear Prediction of Speech* . Springer-Verlag, 1976.

[Mey85] Meyer Y. Principe dínncertitude, bases hilbertiennes et algebres dóperateurs. *Seminaire Bourbaki*, 1985.

[Nav93] Naveen T. and Woods J.W. Subband Finite State Scalar Quantization. *Proceedings, IEEE Int. Conf. Acoust., Speech and Signal Proc.*, pages V.613–V.616, Apr. 1993.

[Ort70] Ortega, J.M. and Rheinboldt. *Iterative Solution of Nonlinear Equations in Several Variables* . Academic Press, 1970.

[Pea90] Pearlman W. A. Adaptive Cosine Transform Image Coding with Constant Block Distortion. *IEEE Trans. Commun.*, pages 698–703, May 1990.

[Ram86] Ramamurthi B. and Gersho A. Classified Vector Quantization of Images. *IEEE Trans. on Com.*, pages 1105–1115, Nov. 1986.

[Ran92] Ran X. and Farvardin N. A Perceptually Motivated Three-Component Image Model - Part II: Applications to Image Compression. *submitted to IEEE Trans. Image Proc.*, July 1992.

[Ris91] Riskin E. A. Optimal Bit Allocation via the Generalized BFOS Algorithm. *IEEE Trans. Inf. Theory*, pages 400–402, Mar. 1991.

[Sha93] Shapiro J.M. Embedded Image Coding Using Zerotrees of Wavelet Coefficients. *IEEE Trans. Signal Proc.*, pages 3445–3462, Dec. 1993.

[Sho88] Shoham Y.; Gersho A. Efficient Bit Allocation for an Arbitrary Set of Quantizers. *IEEE Trans. Acoust. Speech and Signal Proc.*, pages 1445–1453, Sep. 1988.

[Sri92] Sriram P. and Marcellin M.W. Wavelet Coding of Images Using Trellis Coded Quantization. *Proceedings, SPIE Conf. on Visual Commun. and Image Proc.*, Apr. 1992.

[Tan92] Tanabe N. and Farvardin N. Subband Image Coding Using Entropy-Coded Quantization over Noisy Channels. *IEEE J. Select. Areas in Com.*, pages 926–943, June 1992.

[Tru81] Trushkin A. V. . Optimal Bit Allocation Algorithm for quantizing a random vector. *Problems of Inf. Transmission*, pages 156–161, 1981.

[Woo86] Woods J.W. and O'Neil S.D. Subband Coding of Images. *IEEE Trans. Acoust., Speech and Signal Proc.*, pages 1278–1288, Oct. 1986.

[Woo92] Woods J.W. and Naveen T. A Filter Based Bit Allocation Scheme for Subband Compression of HDTV. *IEEE Trans. Image Proc.*, pages 436–440, July 1992.